Differential reddening in 48 globular clusters: An end to the quest for the intracluster medium

E. Pancino[1], A. Zocchi[2], M. Rainer[1,3], M. Monaci[4], D. Massari[5], M. Monelli[6], L. K. Hunt[1], L. Monaco[7], C. E. Martínez-Vázquez[8], N. Sanna[1], S. Bianchi[1], P. B. Stetson[9]

ArXiv 2404.05548

Chromosome maps of globular clusters from wide-field ground-based photometry

S. Jang,[1,2★] A. P. Milone,[1,3] M. V. Legnardi,[1] A. F. Marino,[3,4] A. Mastrobuono-Battisti,[5,6] E. Dondoglio,[1] E. P. Lagioia,[1] L. Casagrande,[7,8] M. Carlos,[1] A. Mohandasan,[1] G. Cordoni,[1] E. Bortolan[1] and Y.-W. Lee[2]

MNRAS 517, 5687-5703 (2022)

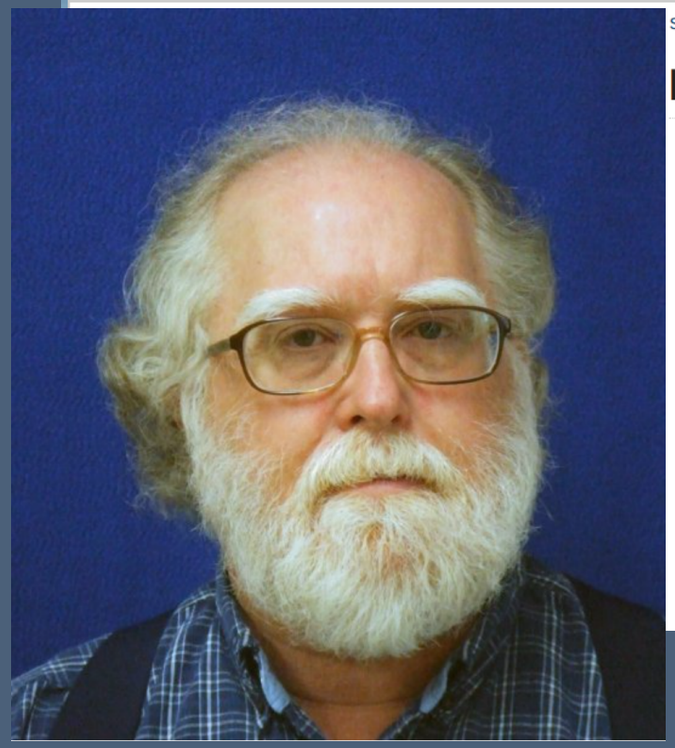

Homogeneous photometry

- Carina
- Fornax
- Leol
- NGC104
- NGC188
- NGC4147
- NGC5904
- NGC6121
- NGC6397
- NGC6791
- Homogeneous UBVRI photometry for 48 globular clusters (MNRAS, 2019 accepted)
- Latest photometry for targets with at least BVI

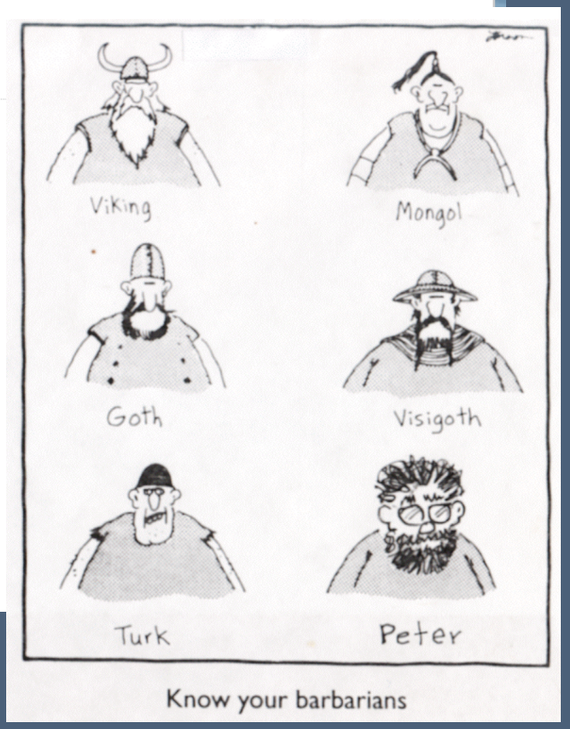

Homogeneous Photometry of 48 globular clusters
by
P. B. Stetson

Monthly Notices
of the
ROYAL ASTRONOMICAL SOCIETY

MNRAS **485,** 3042–3063 (2019)
Advance Access publication 2019 March 2

doi:10.1093/mnras/stz585

Homogeneous photometry – VII. Globular clusters in the *Gaia* era

P. B. Stetson,[1★] E. Pancino,[2,3★] A. Zocchi,[4] N. Sanna[2] and M. Monelli[5,6]

[1] *Herzberg Astronomy and Astrophysics, National Research Council, 5071 West Saanich Road, Victoria, British Columbia V9E 2E7, Canada*
[2] *INAF – Osservatorio Astrofisico di Arcetri, Largo Enrico Fermi 5, I-50125 Firenze, Italy*
[3] *Space Science Data Center, ASI, via del Politecnico snc, I-00133 Roma, Italy*
[4] *European Space Research and Technology Centre (ESA/ESTEC), Keplerlaan 1, 2201 AZ Noordwijk, the Netherlands*
[5] *Instituto de Astrofísica de Canarias, Calle Via Lactea, E-38205 La Laguna, Tenerife, Spain*
[6] *Universidad de La Laguna, Dpto. Astrofísica, E-38206 La Laguna, Tenerife, Spain*

Differential Reddening

Aquila South

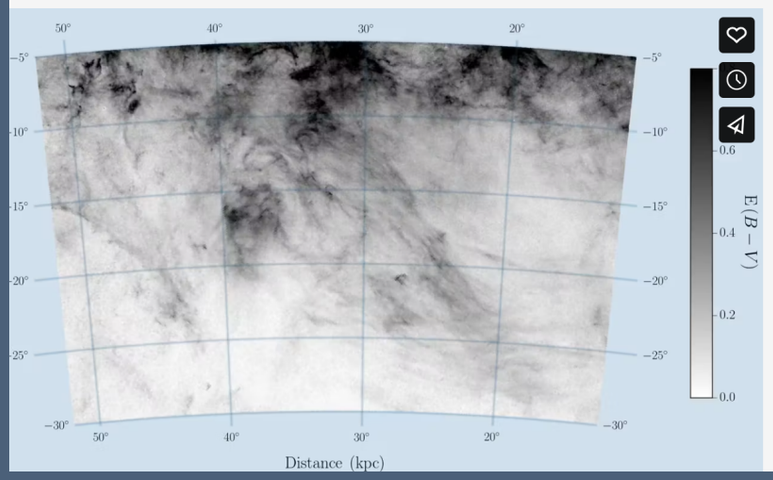

Galactic Plane

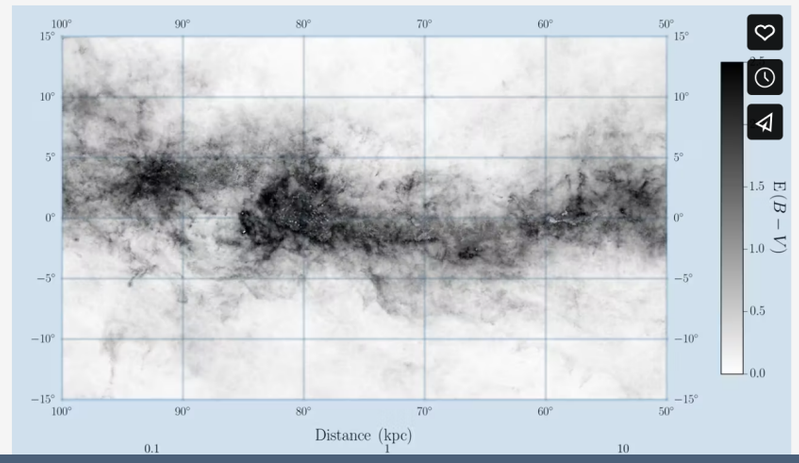

Galactic Anticenter

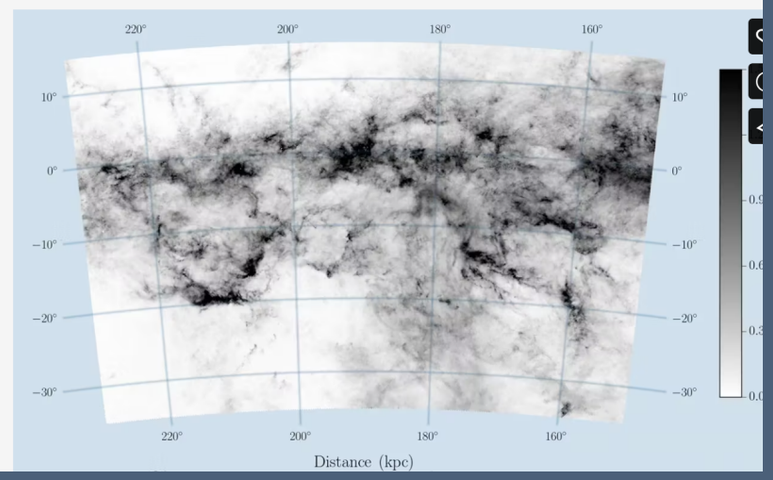

3D Dust Mapping based on Pan-STARSS1, 2MASS, GAIA (http://argonaut.skymaps.info/)

Why is the knowledge of reddening important?

"Interstellar dust attenuates ultraviolet, optical and near-infrared light.
Because the extent of this attenuation is wavelength-dependent,
dust both dims and reddens the light of stars and galaxies before reaching our telescopes"

1. Differential Reddening in 48 Globular Clusters

An end to quest for intracluster medium (ICM)

ICM = gas + dust

Globular Clusters (GC) are expected to host a negligible amount of ICM. This is why “average”, “total”, and “foreground” reddening have become fully interchangeable when referring to GCs

Globular clusters are indeed expected to lose their natal gas early (within 3 Myr)

But slow stellar winds (10-20 Km/s) of bright red giants are expected to accumulate in GC cores between subsequent Galactic disk crossings. At each disk crossing, the medium is expected to be removed by ram-pressure stripping

Thus in old (>10 Gyr) GCs with central escape velocities as high as ~90 km/s a thin but detectable ICM of ~10^{-3} – 10^{-1} $M_\odot$ of dust and ~10^{-3} – 10 $M_\odot$ of gas is expected, depending on the GC total mass and on when the last disk crossing occurred

Why is it important to study the ICM?

1. Evolution of stars strictly linked to the embedding medium: regulation of astrochemical processes and the thermal and dynamic state of the system.

2. **Dust** and **gas** affects the overall evolution, and the processes involved are different in the diffuse medium of the Galaxy, GCs, and open clusters

What are the properties of the ICM and which mechanisms are able to remove it during the evolution of a star cluster?

Observations

50 years of observations of GC cores, using a variety of techniques provided mostly upper limits to the ICM content, which are all a few orders of magnitude smaller than expected on the basis of stellar evolution theory and mass loss among bright red giants

Only a few detections of dust or gas claimed so far: NGC 362, NGC 2808, NGC 6624, NGC 7078 (M 15), and NGC 104 (47 Tuc)

1. NGC 362 and NGC 6624: photometric detections based on the presence of dark patches and on the color and polarimetry of optical data
2. NGC 2808: HI detection not securely associated to the GC
3. NGC 6624: Hα detection of ionized gas
4. M 15: **dust** detected through its thermal emission in the infrared with Infrared Space Observatory
5. 47 Tuc: ionized **gas** was detected through the study of its pulsars

N. B. In the literature data, detections either compatible or only marginally inconsistent with the mentioned ICM production expectations

Inconsistency between observations and expectations is related to the upper limits in the literature while not affecting the few actual detections

How to study the (presence of) ICM ?

Differential Reddening

Color-Magnitude Diagram

A. Mean Ridge Line (MRL)

B. Color excess w.r.t. the MRL

C. Map of DR variations across the FoV

Methodology

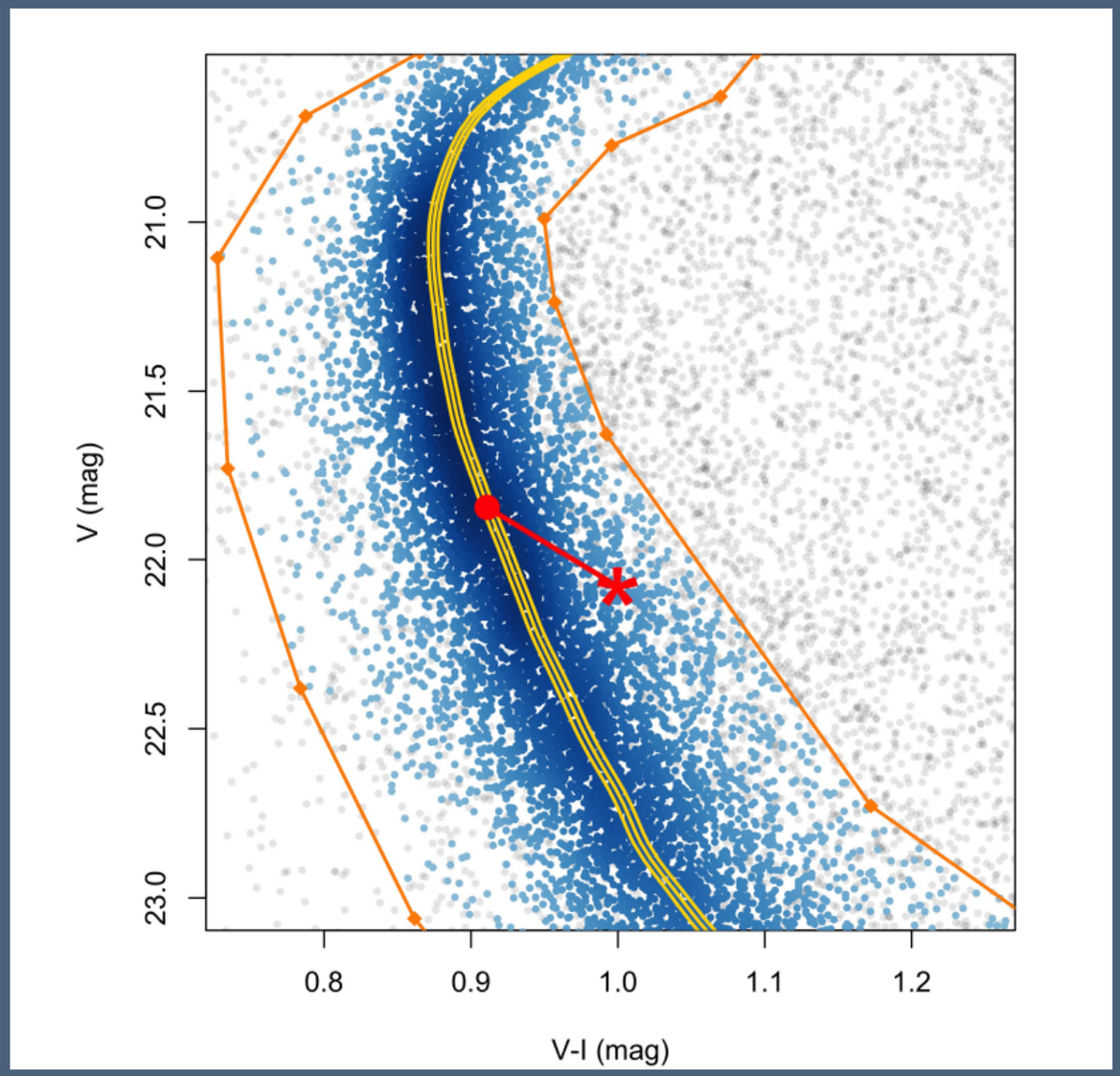

IC 4499

- Photometric quality parameter selection
- Choice of particular band combinations
- Exclusion of specific features in the CMD (photometric binaries)
- Spatial smoothing (smoothing in sky coordinates so to make the spatial reddening variations emerge from the noise of photometric uncertainties)
- Assumptions on the reddening law Rv = 3.1 $A_V = R_V/E(B-V)$

Methodology

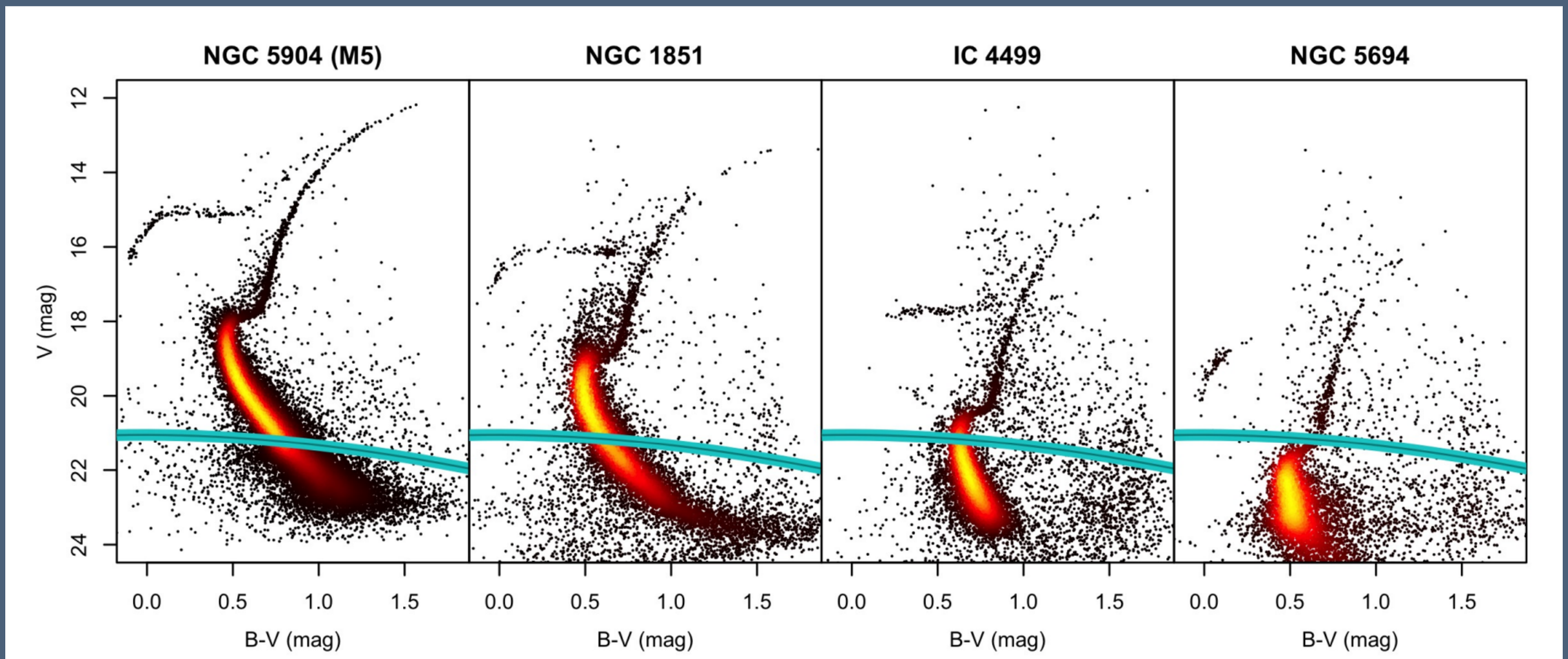

Fig. 1. Examples of color-magnitude diagrams from Stetson et al. (2019), for GCs at different distances. The *Gaia* limiting magnitude (G≃21 mag) is plotted in all panels as a dark cyan line, with its uncertainty interval in cyan, based on the color transformations by Pancino et al. (2022).

Proper Motion Selection (?)

Methodology

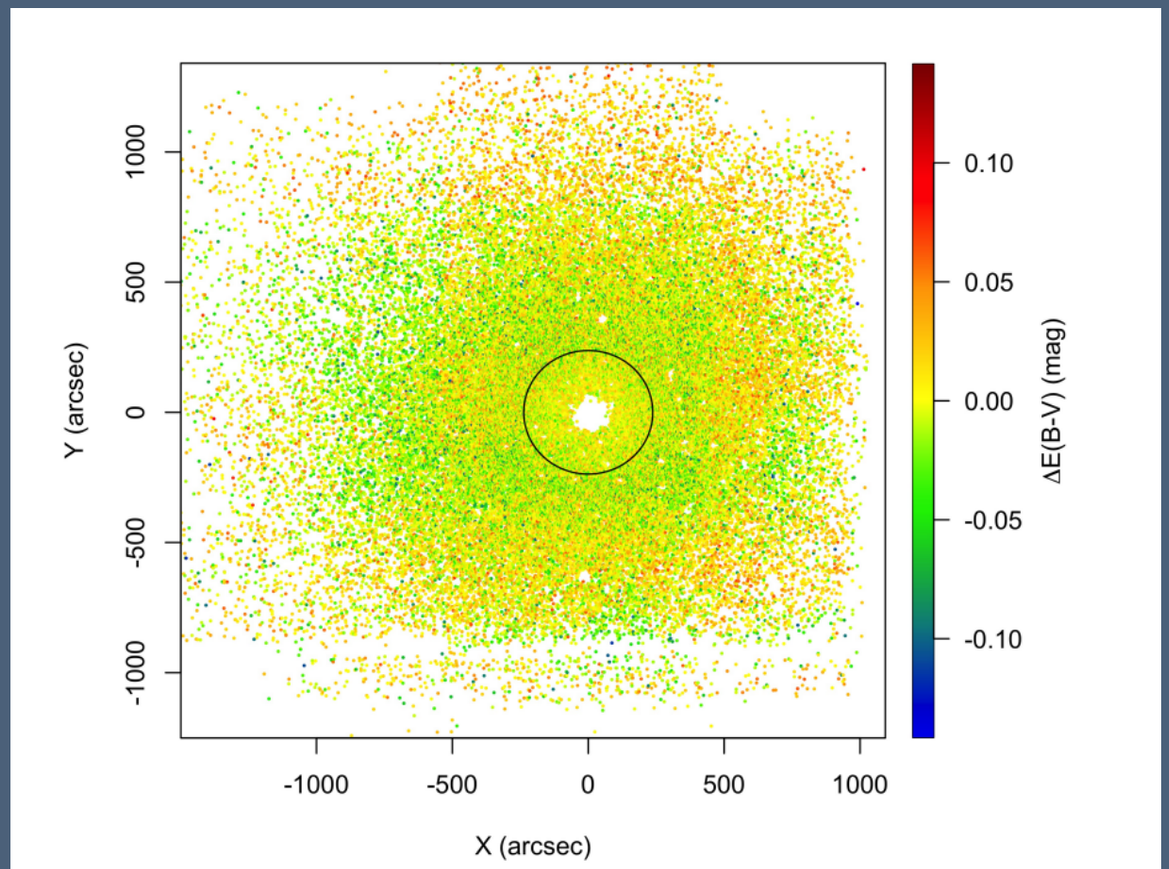

Fig. 4. Example of (raw) DR map dominated by instrumental features, in the case of NGC 104 (47 Tuc). The footprint of the CCD frames included in the original wide field photometry (Stetson et al. 2019) is clearly visible. The half-light radius (r_h) is plotted for reference. The hole in the GC center is caused by stellar crowding.

47 Tuc FoV "square" features

Zero Point variations

A. Non homogeneous sensitivity of the chip

B. Non uniform readout

C. FoV distortion

D. Concentration of light

Methodology

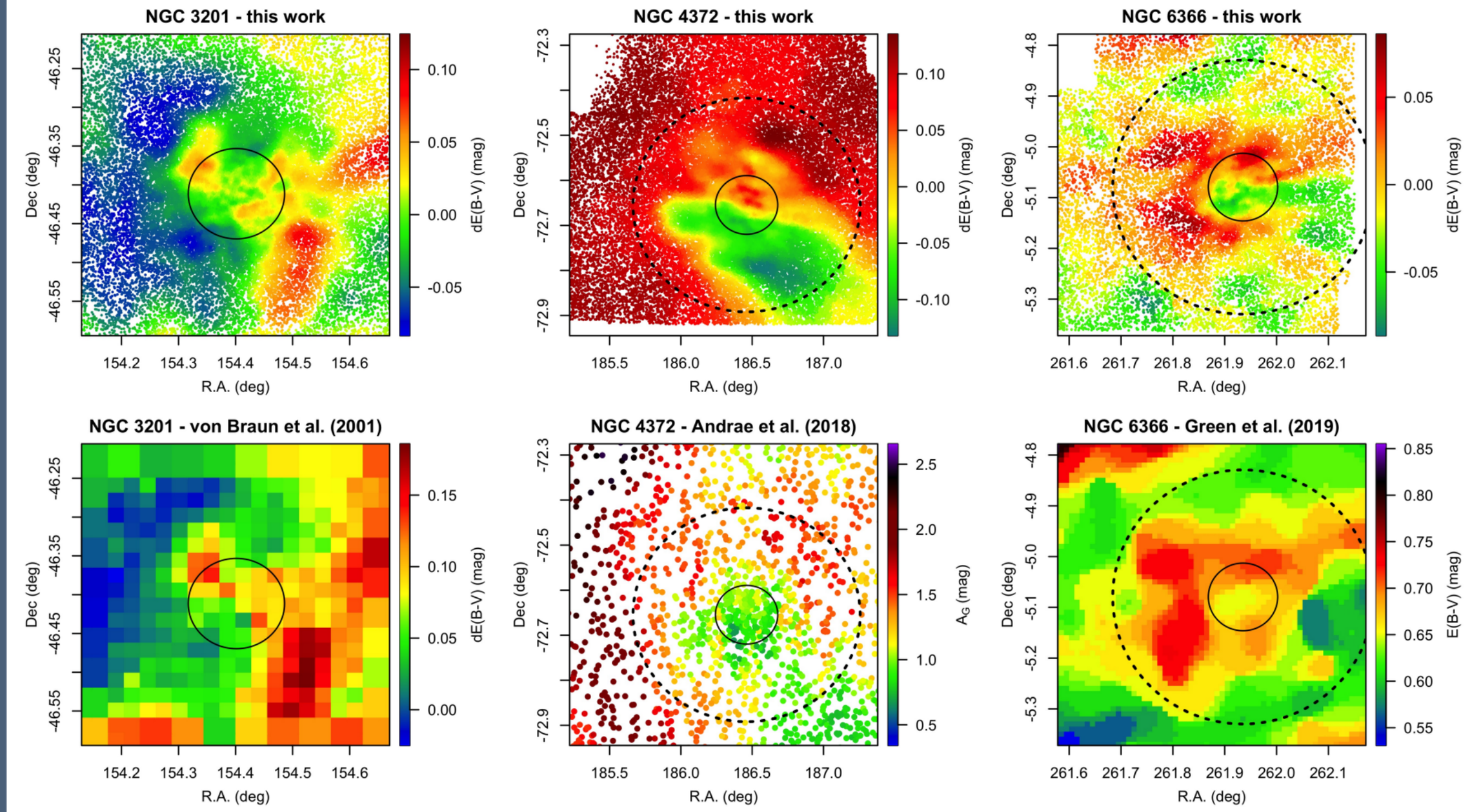

Fig. 3. Comparison of our DR maps (top row) with literature ones (bottom row) for three well-studied GCs, as annotated. The left panels show

CMDs corrected for differential reddening

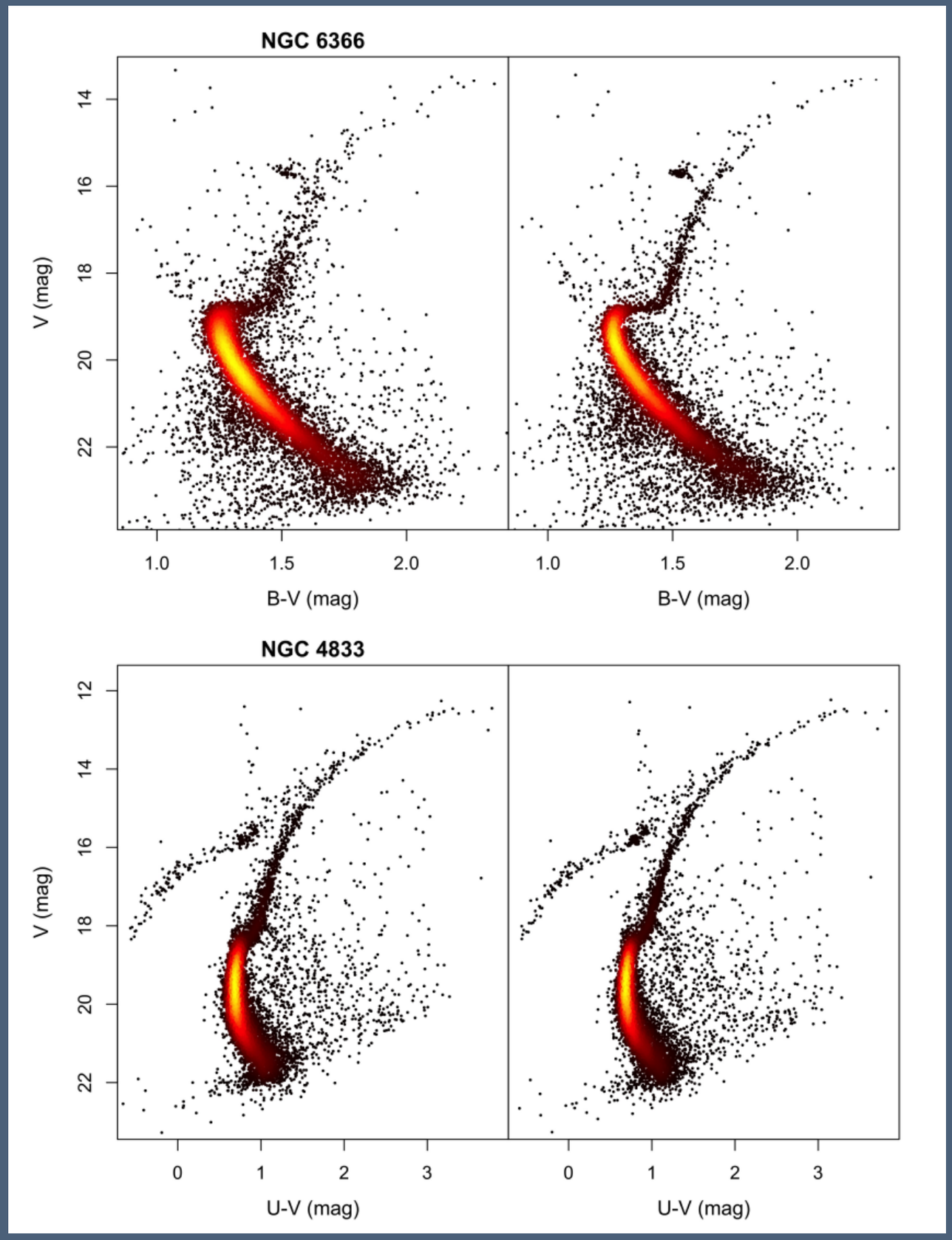

Flat Trend

- If DR_{max} of GCs with low E(B-V) or high B were entirely caused by foreground dust, we would expect them to correlate with the total amount of reddening, but weak or no correlation is found with different correlation rank tests

- observed a systematic increase in the DR_{max} with the total area covered by GC: if the DR were caused entirely by the foreground medium, such as for example a filament passing in front of the GC, we would not expect any systematic variation of the total DR with the area covered within each GC

Galactic cirri are visible at all latitudes, they contain gas (atomic and molecular) and dust, and are mostly located within a few hundred parsecs from the Sun. They have typical widths of the order of 0.1 pc and their projected width is 3 - 4 arcmin for a typical distance of 100–200 pc

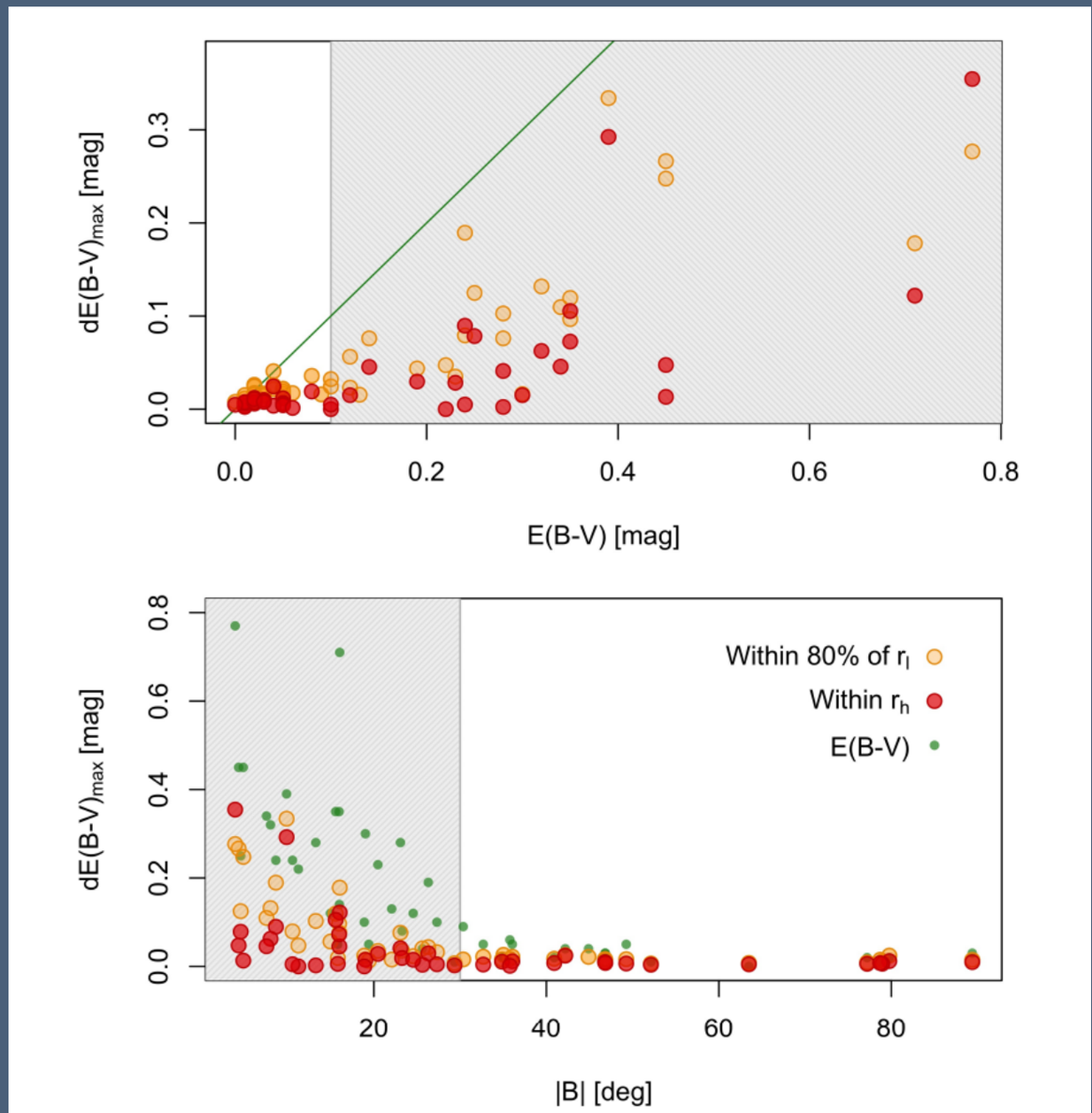

Fig. 7. Behavior of the total DR, $dE(B–V)_{max}$, with E(B–V) (top panel) and Galactic latitude (bottom panel). In each panel, orange symbols are the total DR computed within 80% of r_ℓ, red ones within r_h. The green line in the top panel is the 1:1 agreement, while the green dots in the bottom panel are the E(B–V) values of the sampled GCs. The gray-shaded areas cover the high-reddening sample (Sect 4.2).

two groups of GCs based on their DR trend

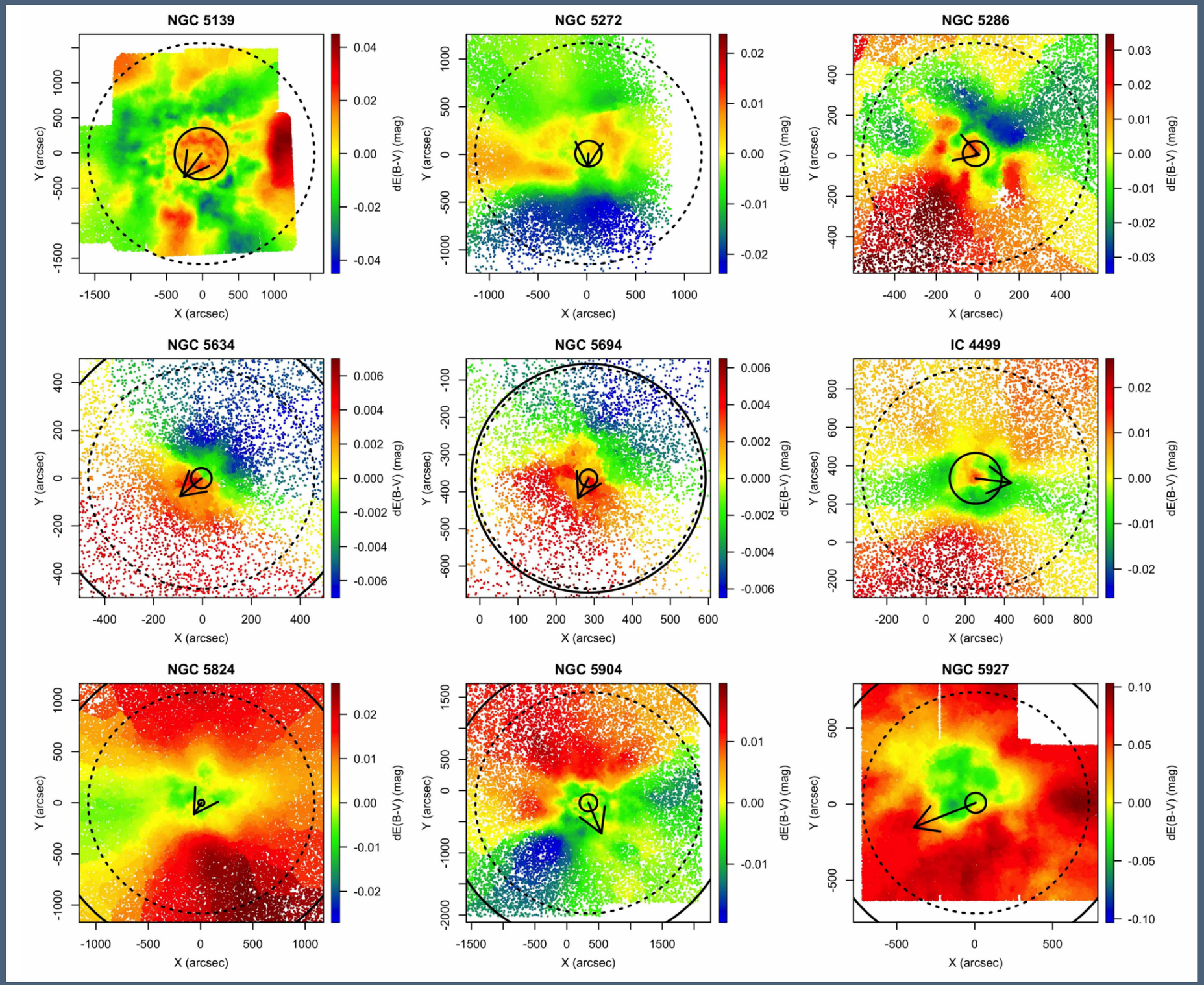

Because substructures are found within the GC half-light radii (typically 4 arcmin extended) of each of the 48 GCs, and because the sky coverage of cirri appears so uneven, it is unlikely that all of the observed substructures in the observed GC sample are caused by the local foreground medium of the Milky Way

Selection of GCs

Of the 48 GCs in our sample, 33 are contaminated or suspected to be contaminated by foreground medium, 4 are not obviously contaminated, but belong to the high-reddening sample, and...11 appear to be clean from any foreground contamination. It is worth emphasizing at this point that if a GC is contaminated by foreground medium, this does not automatically exclude the presence of an appreciable ICM, it just makes it difficult to separate the ICM (if any) from the foreground contamination. A chief example is M 3, which has a foreground contamination of about 0.01 mag, while (DR) maps show reddening variations of about 0.03 mag. Clearly...DR maps cannot be directly used on M 3, even if the observed DR cannot be entirely explained by foreground contamination, but... can use this information to attempt a statistical decontamination.

It is interesting to note that of the 11 clean GCs, 10 are associated to streams of disrupted dwarf galaxies in the Galactic halo...this could be due to a selection bias...high latitude Galactic regions are less likely to be contaminated by dust, and high-latitude GCs typically move on eccentric orbits that keep memory of their accreted origin. ... accreted GCs are the best candidates to have retained gas and dust within their potential well. In fact, the interactions and shocks they experienced with the Galaxy are less in number (their orbits cross the disk less frequently because of the larger periods) and are less intense due to the dark matter halo of the progenitor galaxy that shields them, at least until its disruption.

Theoretical predictions of ICM mass

$$M_{gas} = \frac{\tau_c}{\tau_{HB}} N_{HB}\, \delta M_{HB}$$

where τ_c is the time since the last Galactic disk crossing, τ_{HB} the typical lifetime of the horizontal branch (HB) stars, N_{HB} the number of HB stars in each GC, and δM_{HB} the typical mass lost by stars before the HB.

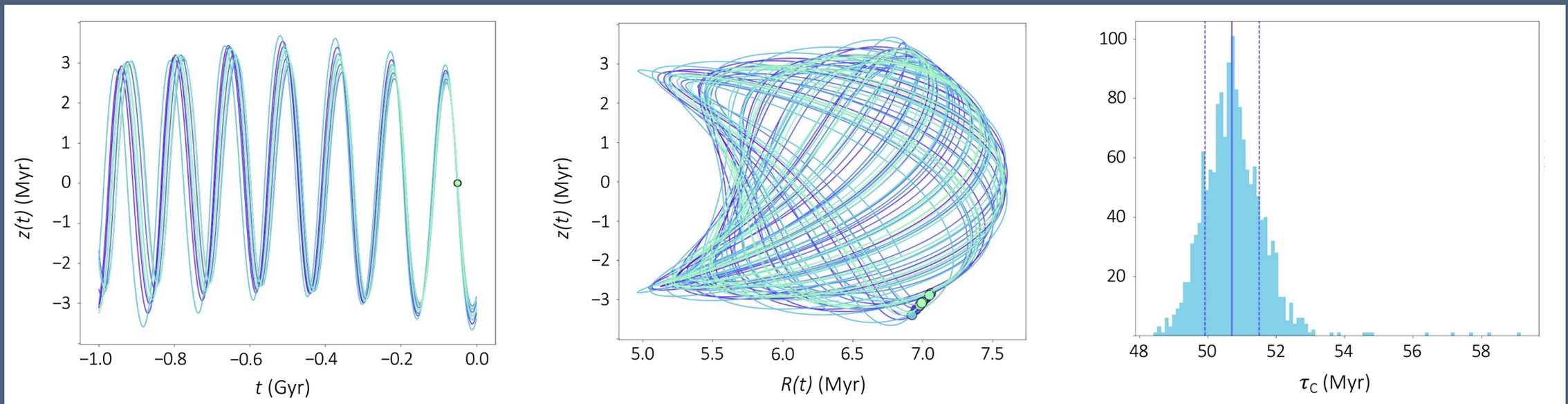

Fig. 8. Example of the orbital computation and determination of τ_c for NGC 104 (47 Tuc). Variation of the height above the Galactic plane as a function of time (leftmost panel) and galactocentric radius (center panel), for ten randomly selected orbits out of 1500 realizations. The starting point of each orbit integration is plotted as a dot with the same color of the corresponding orbit. The rightmost panel shows the distribution of the 1500 resulting τ_c, with its median and MAD as solid and dotted lines, respectively.

Theoretical predictions of ICM mass

$$\frac{M_{dust}}{M_{gas}} = 0.009 \frac{(O/H)}{(O/H)_{\odot}}$$

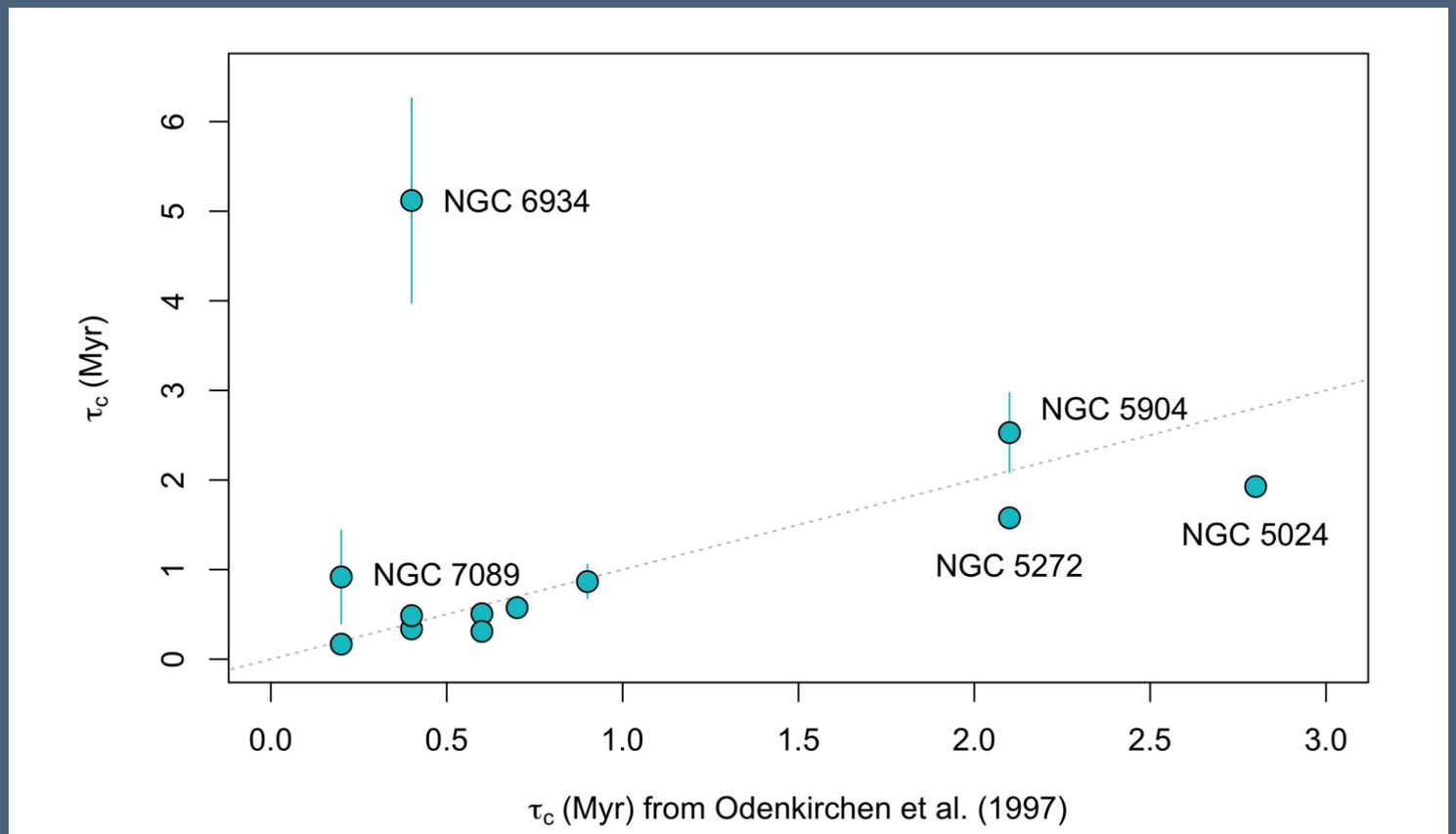

Fig. 9. Comparison between our τ_c estimates and those by Odenkirchen et al. (1997) for 12 GCs in common. Perfect agreement is marked by a dotted line. Errorbars are plotted for each GC, but are mostly smaller than the points. The GCs for which τ_c has changed are labeled.

ICM mass from reddening maps

$$\frac{N_H}{E(B-V)} = 5.94\ (\pm 0.34) \times 10^{21}\ \mathrm{H\,cm^{-2}}$$

" the pulsar timing data in 47 Tuc (Abbate et al. 2018) highly disfavor a concentrated distribution, and thus we considered a homogeneously distributed ICM across the entire GC, within the tidal (truncation) radius"

"It should be emphasized that the direct observation of atomic hydrogen through 21 cm emission is not straightforward. Lynch et al. (1989) tried a deep search (≃16 hrs) in NGC 6388 that resulted in a non-detection, deriving 3.8 $M_\odot$ as an upper limit for the HI mass. Considering a distance of ~ 10 kpc, the column density would be ~ 1.4×10^{18} cm^{-2} , below the detection limit of modern HI surveys (Peek et al. 2018). Furthermore, at 1.42 GHz the beam dilution is not negligible, since the beam size is generally bigger than the GCs angular size, making the detection even more difficult. Faulkner et al. (1991) searched for HI in NGC 2808, finding atomic hydrogen concentrated near the GC center, with the GC systemic velocity, but unknown distance.

HI is nearly ubiquitous in the Galaxy and it is optically thin, so the full line of sight contributes to the observed profile, and the emission from background and foreground gas may pollute the detection, coupled with stray radiation, complicating the picture. The observed profiles are generally complex, formed by multiple components, hard to associate with environments mapped by the line of sight, despite significant effort in this sense ..."

Results

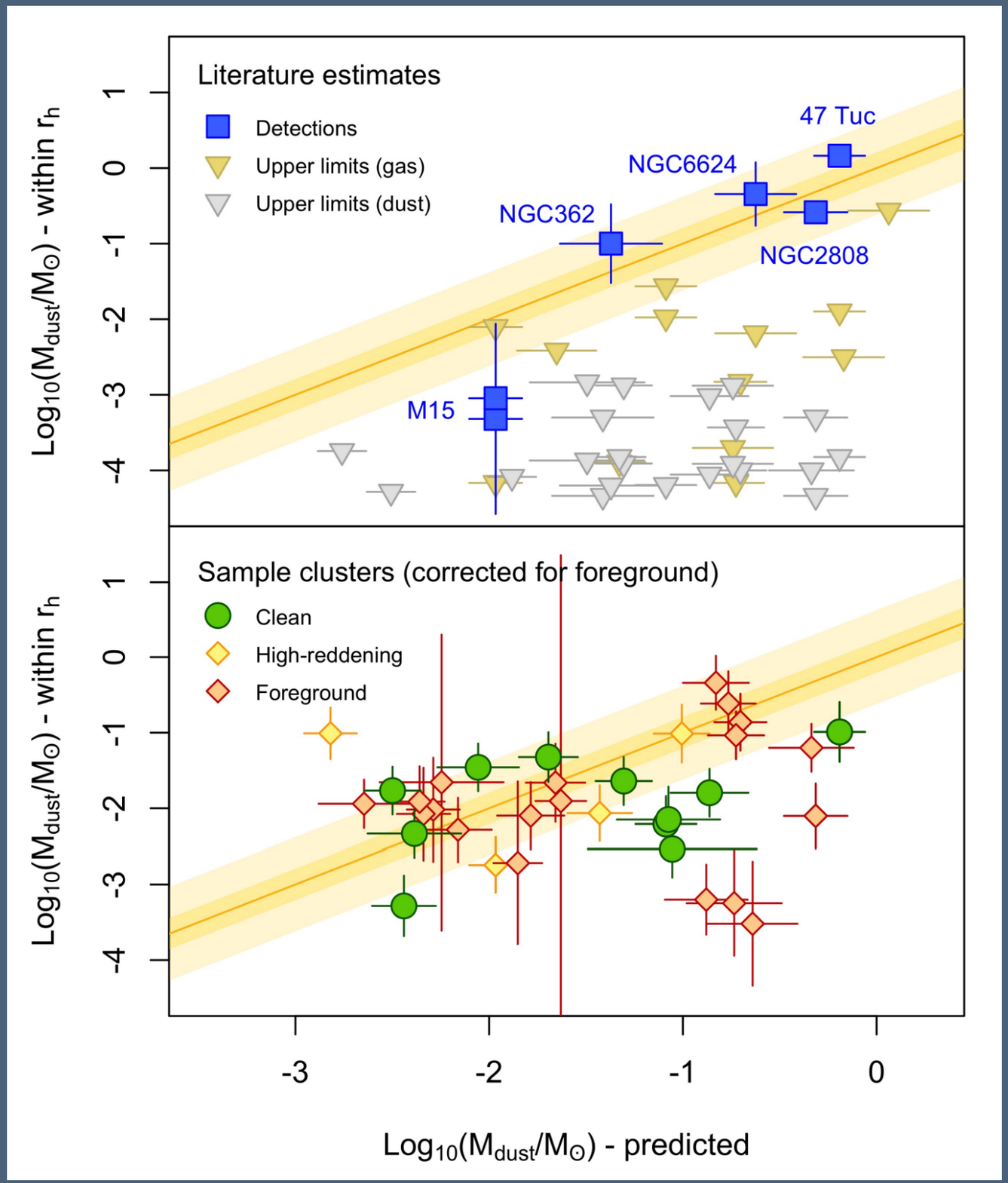
Literature estimates
Detections
Upper limits (gas)
Upper limits (dust)
47 Tuc
NGC6624
NGC362
NGC2808
M15
Sample clusters (corrected for foreground)
Clean
High-reddening
Foreground
Log10(Mdust/M⊙) - within rh
Log10(Mdust/M⊙) - predicted
1
0
-1
-2
-3
-4

Discrepancy culprits

1. ICM spatial distribution
2. Dust/gas or ionization differences
3. Dust composition
4. Dust temperature

2. Chromosome maps of globular clusters from wide field photometry

Globular clusters (GCs) host two main groups of stars: a first stellar population (hereafter 1G) with chemical composition that resembles halo field stars, and a second population (2G) of stars enriched in helium, nitrogen and sodium and depleted in carbon and oxygen

Multiple populations have been widely investigated during the past decades but their origin still represents one of the most intriguing open issues in stellar astrophysics. According to some scenarios, the multiple populations are the signature of multiple star-formation episodes, where 2G stars originate from material polluted by more massive 1G stars

GC stars are coeval and that accretion of polluted material on to pre-MS stars is responsible for the chemical composition of 2G stars.

As an alternative, stellar mergers are responsible for multiple populations in GCs

2. Chromosome maps of globular clusters from wide field photometry

Multiple populations studied with HST through F275W, F336W, F438W, and F814W bands

One of the major limitations is the small field of view of HST cameras, which restricts most of the studies on Galactic GCs to the innermost cluster regions. Clearly, wide-field photometry is mandatory to extend the investigation of multiple populations to the entire cluster.
To overcome the main limitation of HST, ground-based facilities are used to investigate the multiple stellar populations in Galactic GCs by means of photometric diagrams that are sensitive to the chemical composition of the distinct populations. The most-used diagrams involve CMDs and pseudo-CMDs built with Stroemgren photometry, or photometry from appropriate narrow-band filters, or appropriate combinations of the U, B, V and I Johnson-Cousin bands (U, B, I)

Photometric diagrams made with the CU, B, I = (U − B) − (B − I) pseudo-colour, are efficient tools to disentangle stellar populations with different light-element abundances along the red-giant branch (RGB), whereas CMDs made with B − I colour are sensitive to stellar populations with different helium abundances

How to study the (presence of) MPs ?

Differential Reddening

Color-Magnitude Diagram (Local approach)

A. Mean Ridge Line (MRL) in a rotated system

B. Color excess w.r.t. the MRL

C. Map of DR variations across the FoV

Differential Reddening

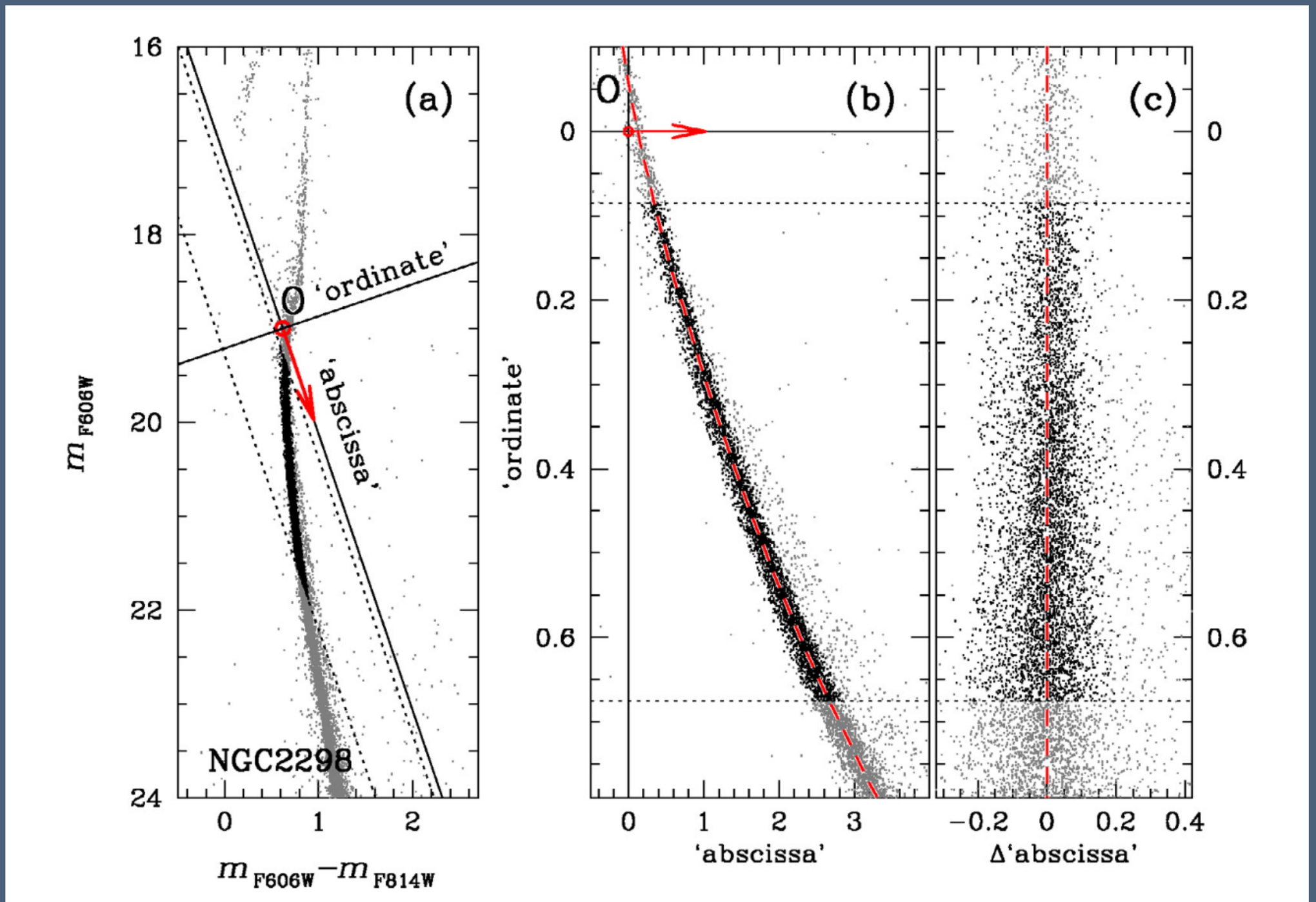

Differential Reddening

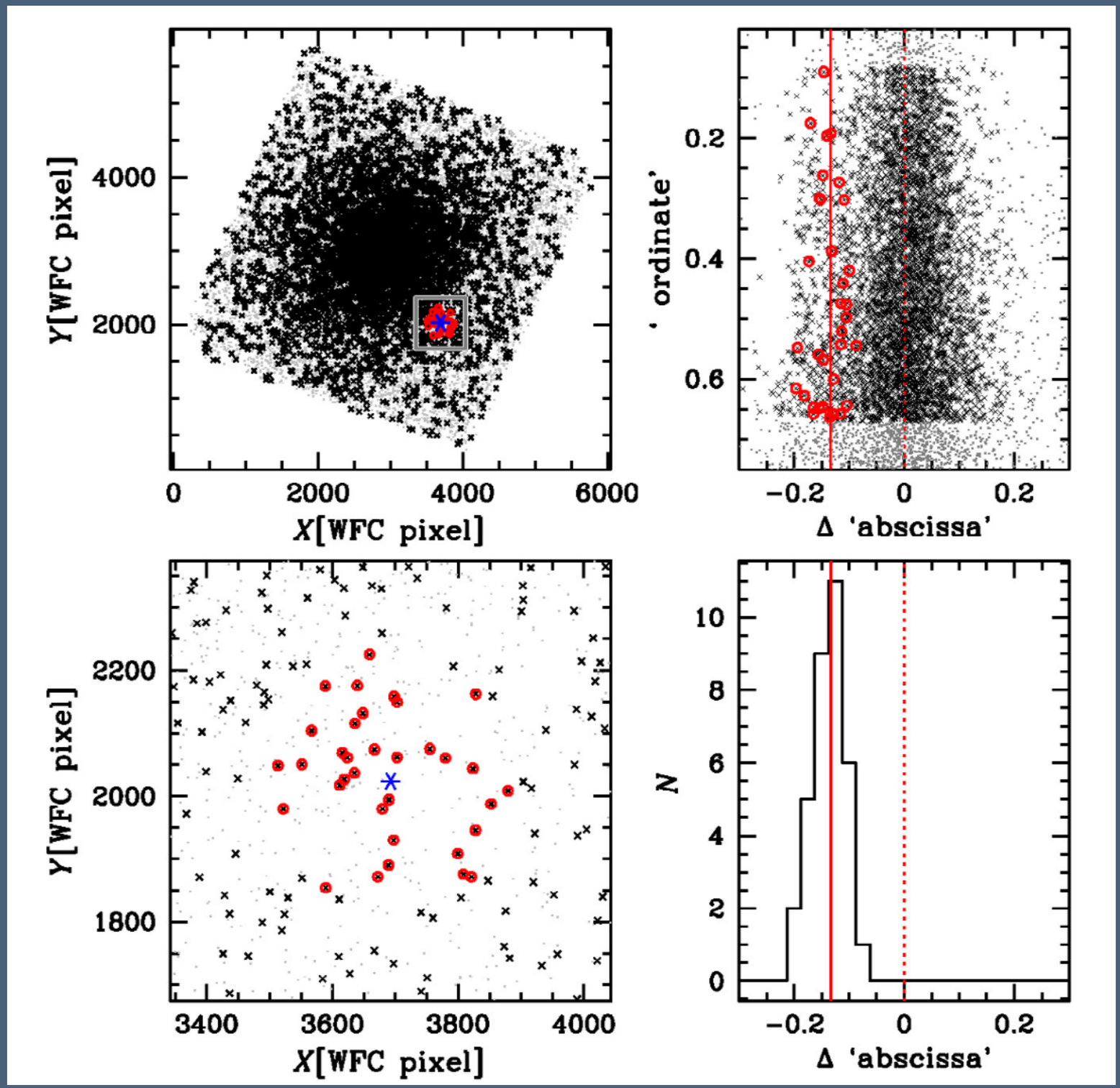

Proper motions: cluster members selection

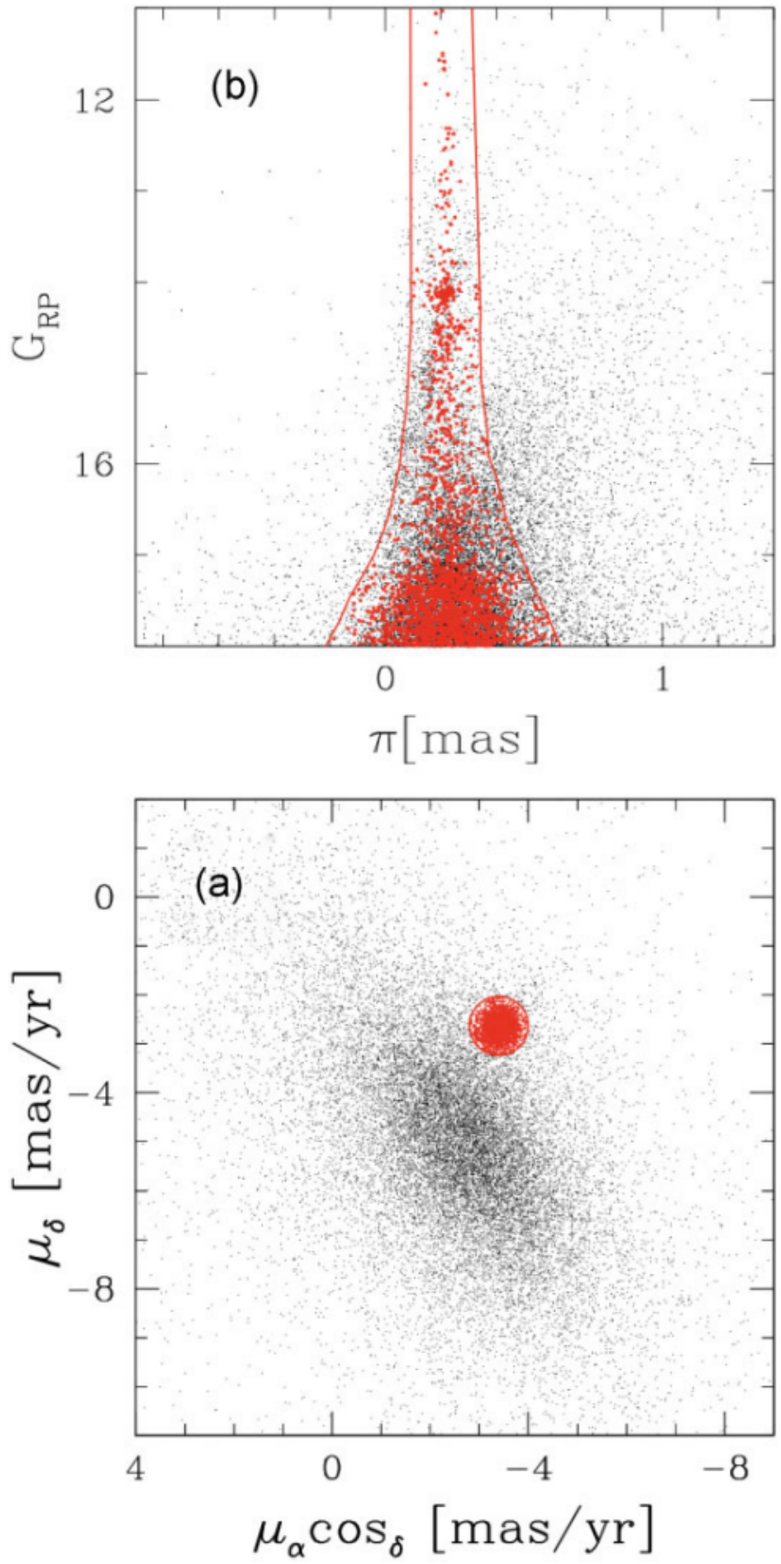

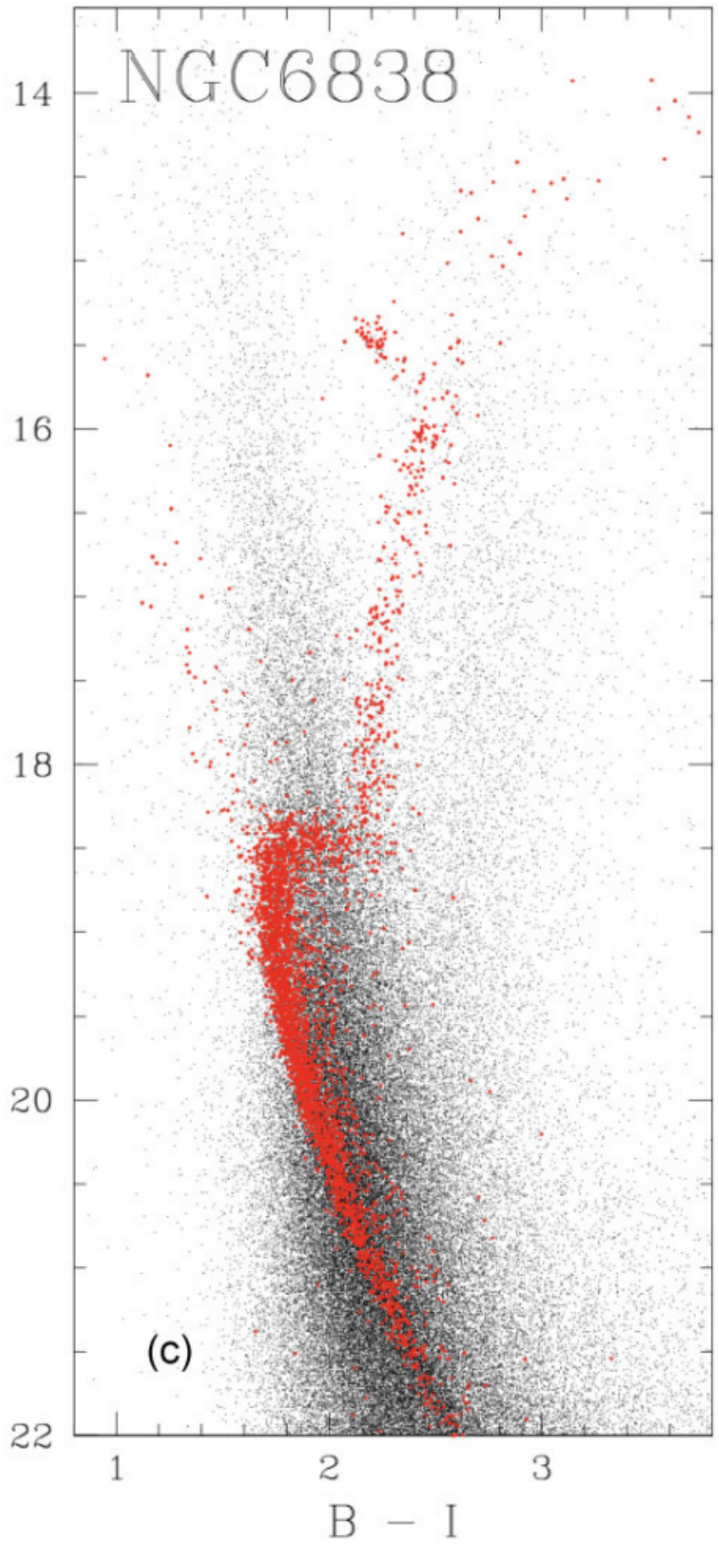

Differential Reddening

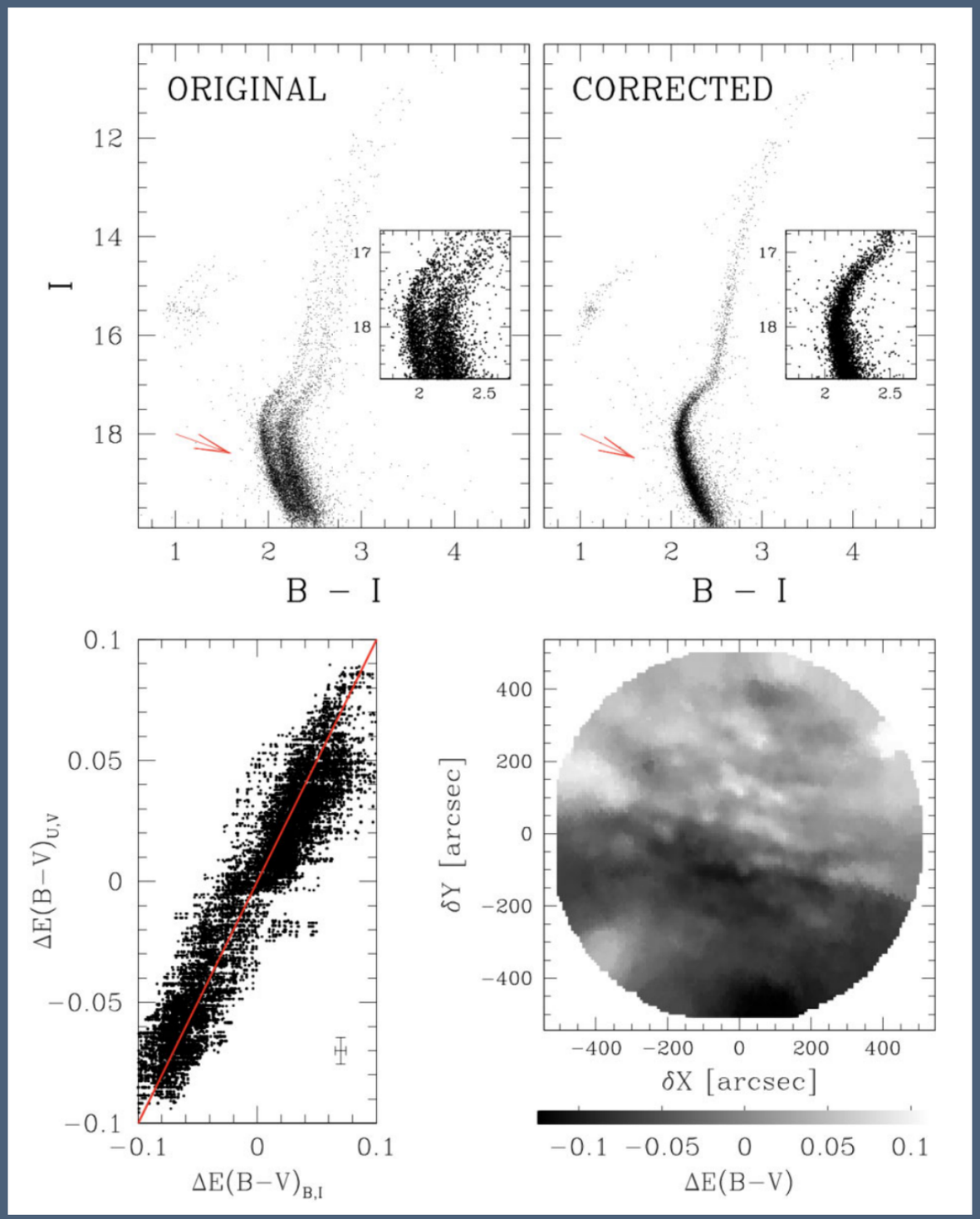

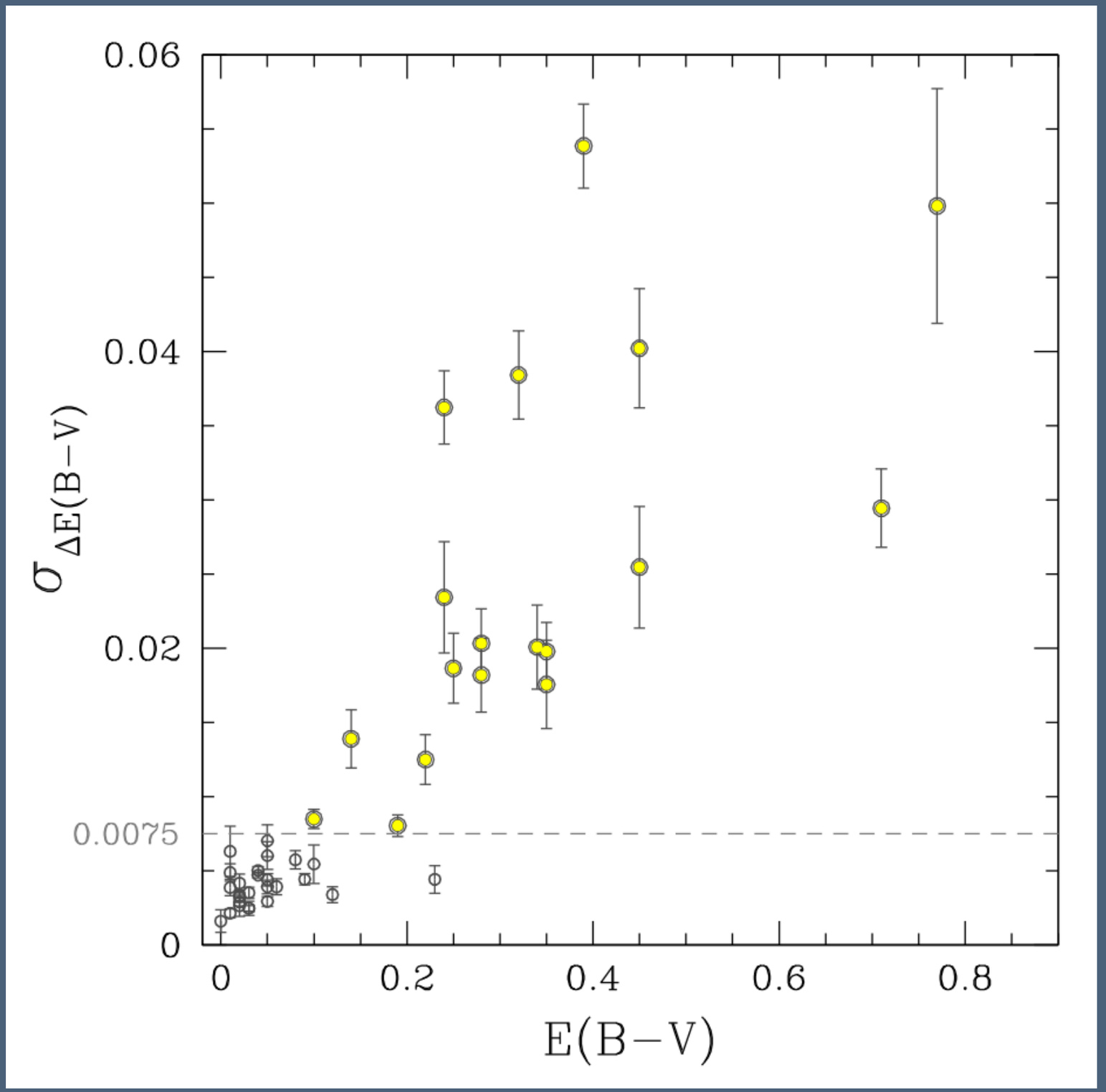

$\sigma_{E(B-V)}$ indicates the 1σ value of average reddening of each of 100 × 100 arcsec cells dividing the field of view of a GC Photometry of 18 GCs with σ E(B − V) > 0.0075 colored in yellow have been corrected for the effect of differential reddening

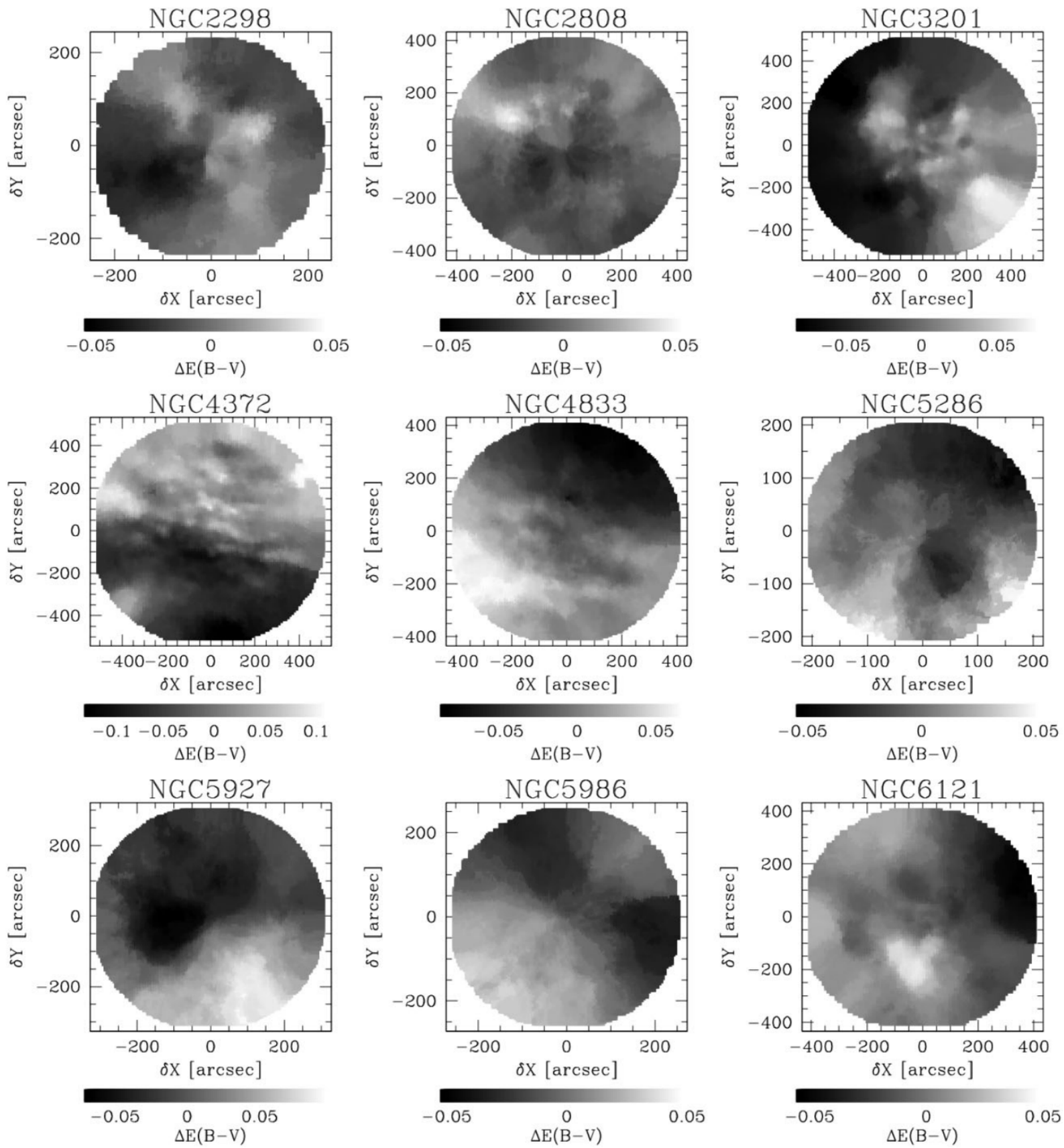
NGC2298
NGC2808
NGC3201
NGC4372
NGC4833
NGC5286
NGC5927
NGC5986
NGC6121
δY [arcsec]
δX [arcsec]
ΔE(B−V)

Chromosome map

$$\Delta_{\mathrm{B,I}} = W_{\mathrm{B,I}} \frac{X - X_{\mathrm{fiducialR}}}{X_{\mathrm{fiducialR}} - X_{\mathrm{fiducialB}}},$$

$$\Delta c_{\mathrm{U,B,I}} = W_{C\mathrm{U,B,I}} \frac{Y - Y_{\mathrm{fiducialB}}}{Y_{\mathrm{fiducialR}} - Y_{\mathrm{fiducialB}}}$$

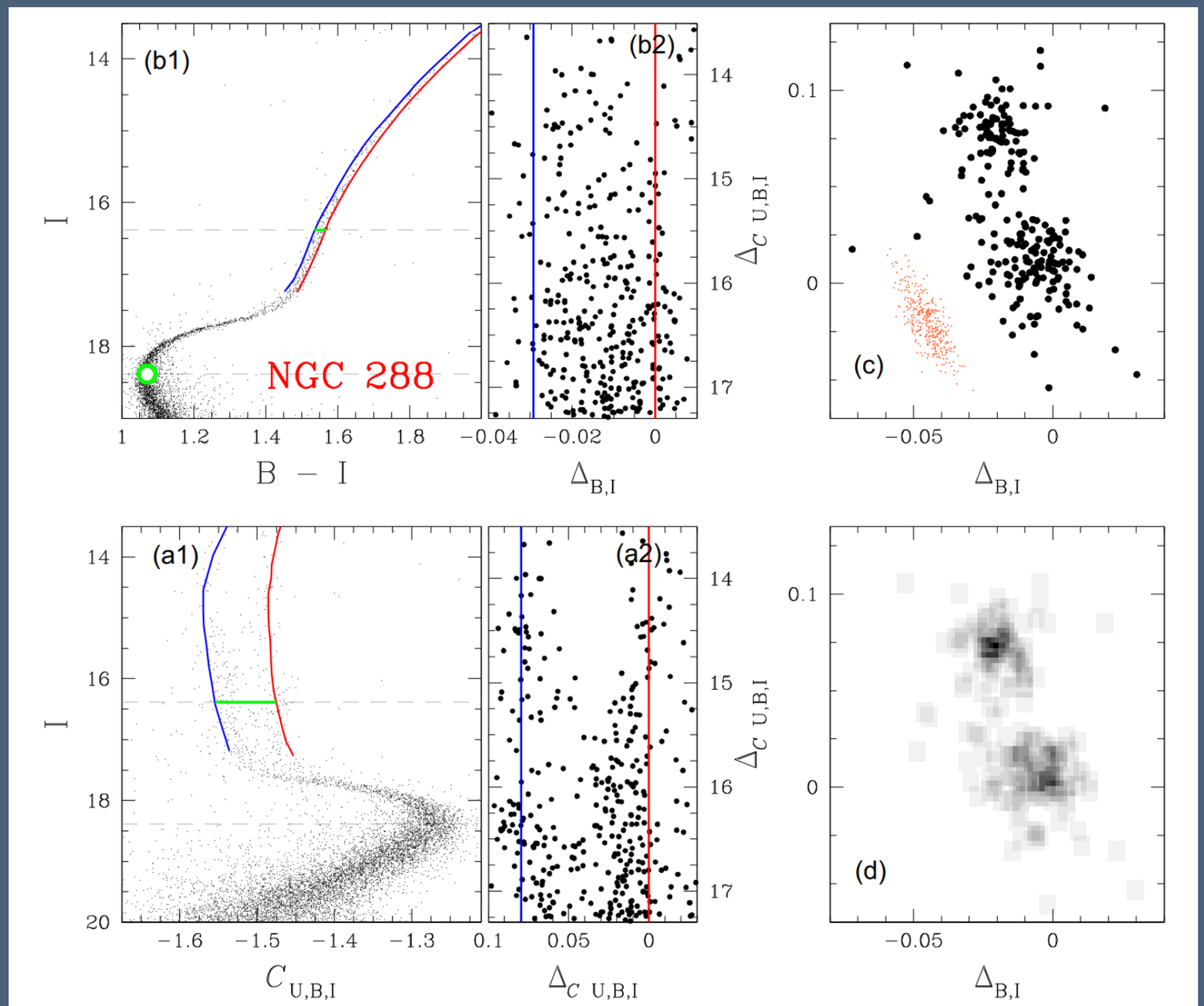

Chromosome map

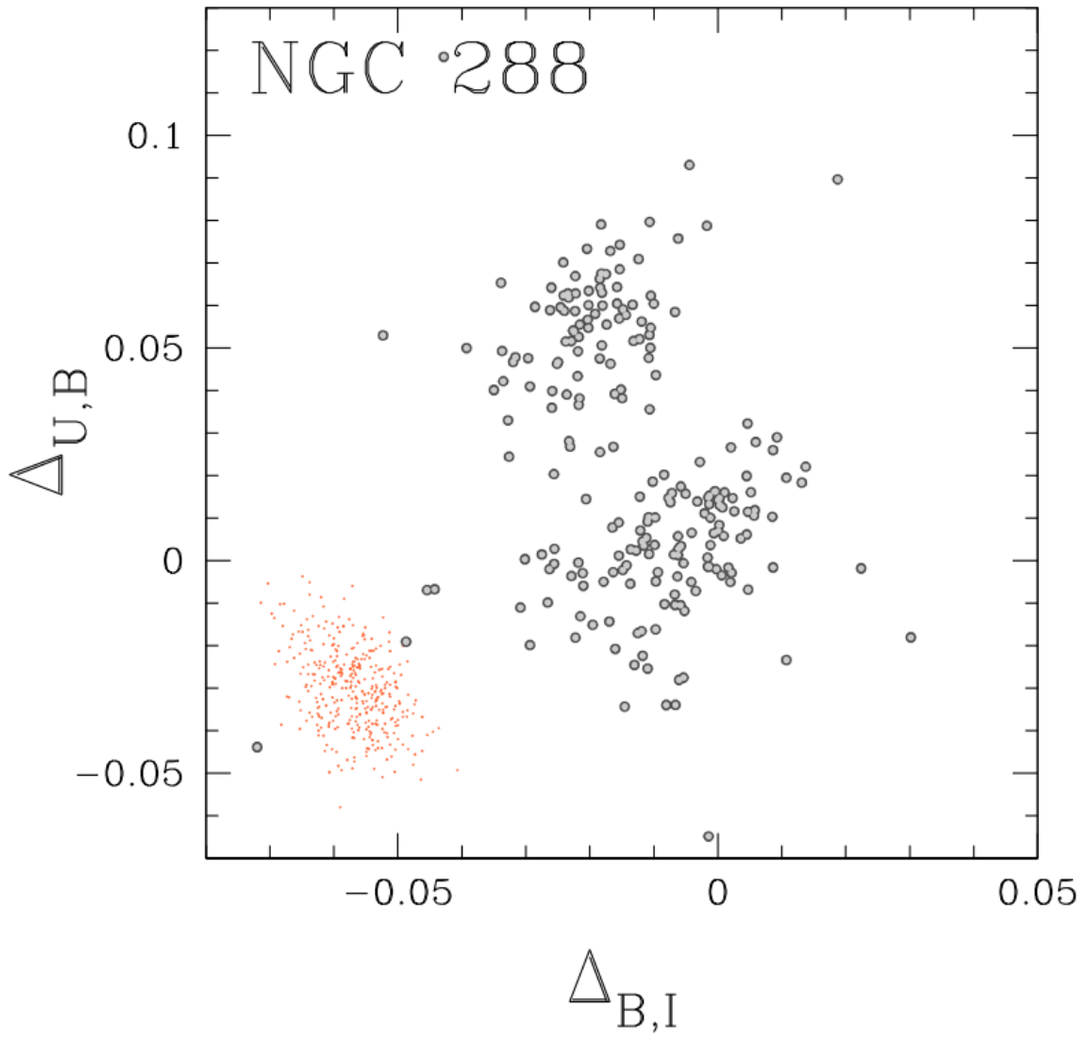

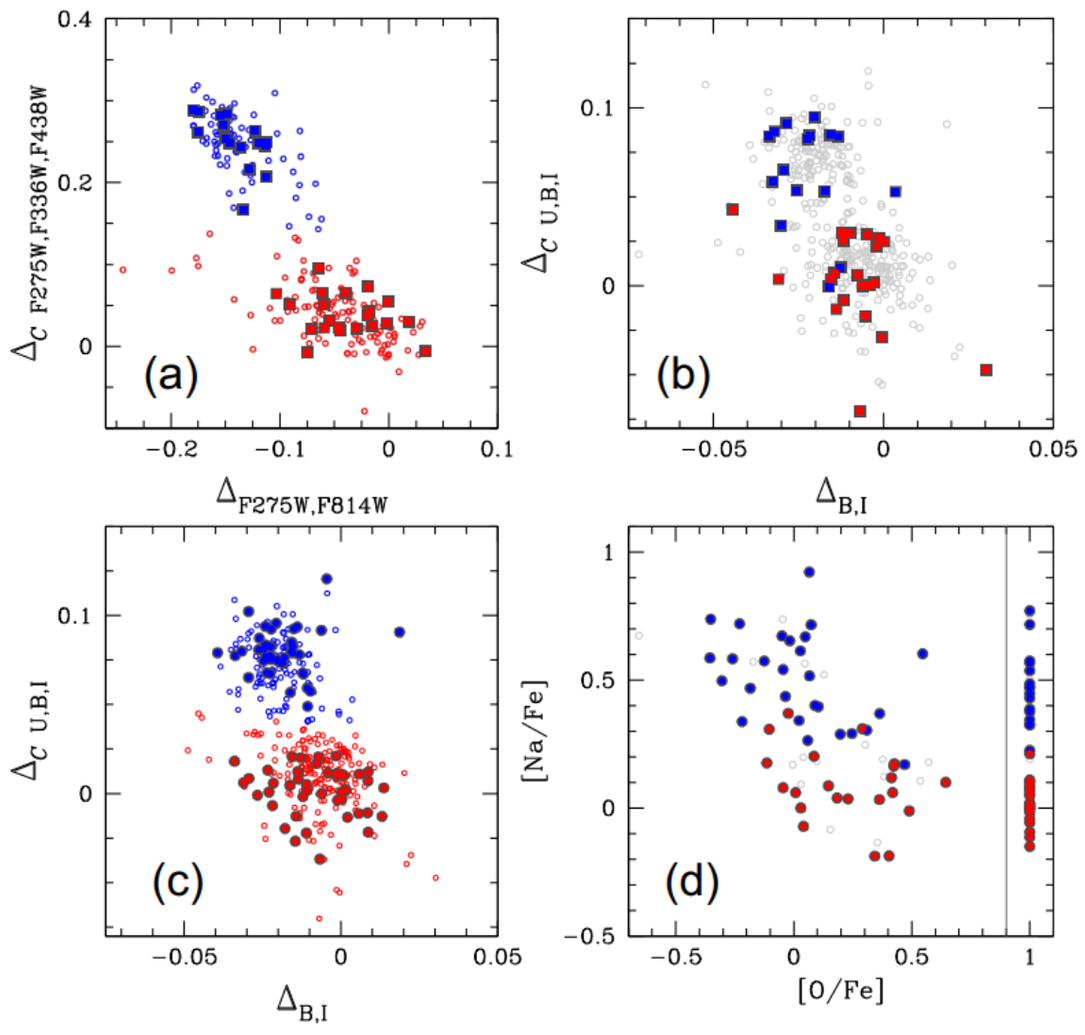

Chromosome map: theoretical predictions

Table 1. Chemical composition of the six isochrones shown in Fig. 9. All isochrones have ages of 13 Gyr and $[\alpha/\mathrm{Fe}] = 0.4$.

Isochrone	Y	(C/Fe)	(N/Fe)	(O/Fe)	(Fe/H)
I1	0.246	0.00	0.00	0.40	−1.50
I2	0.256	−0.05	0.53	0.35	−1.50
I3	0.276	−0.10	0.93	0.20	−1.50
I4	0.306	−0.50	1.21	−0.10	−1.50
I5	0.266	0.00	0.00	0.40	−1.50
I6	0.246	0.00	0.00	0.40	−1.45

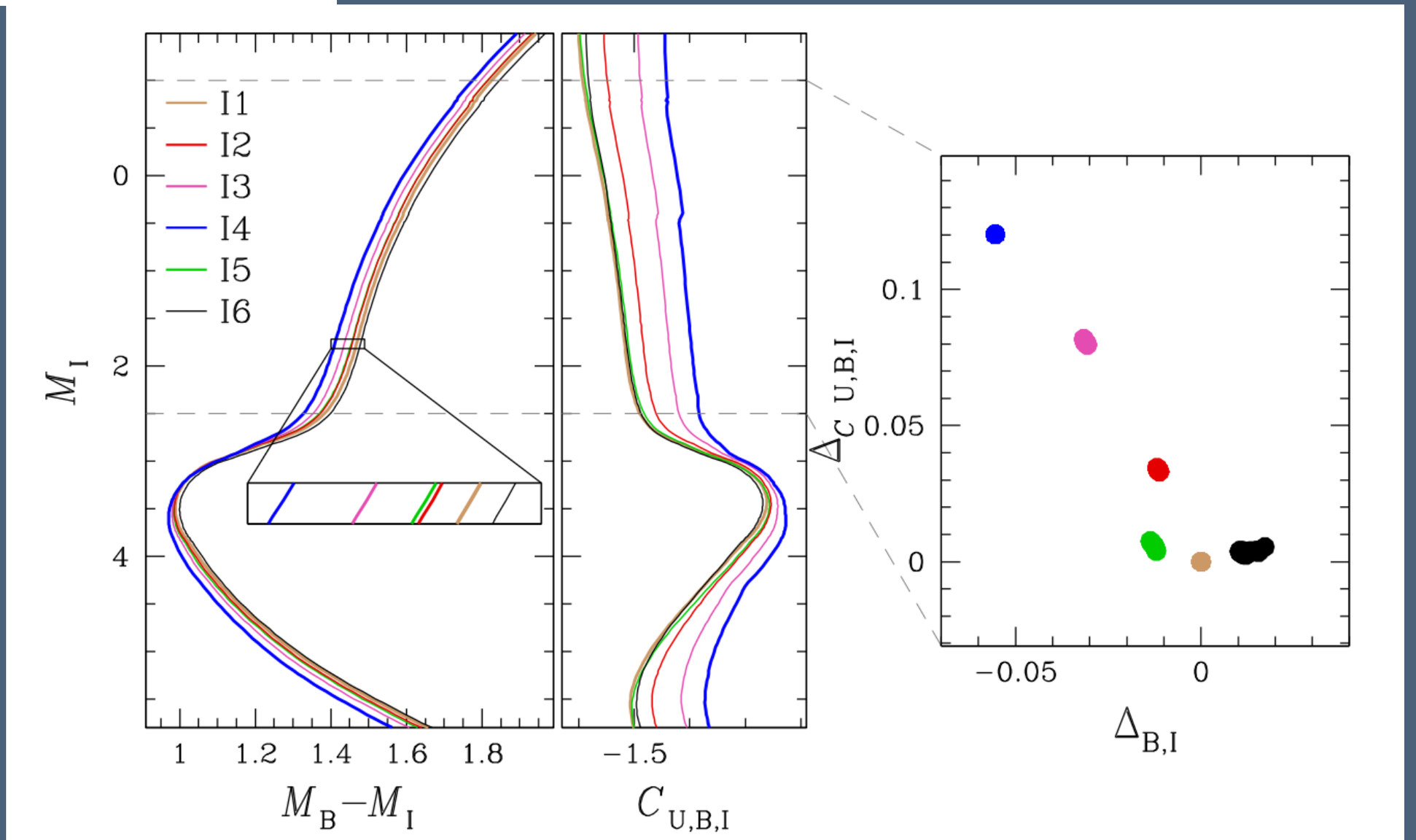

Atlas of Chromosome maps

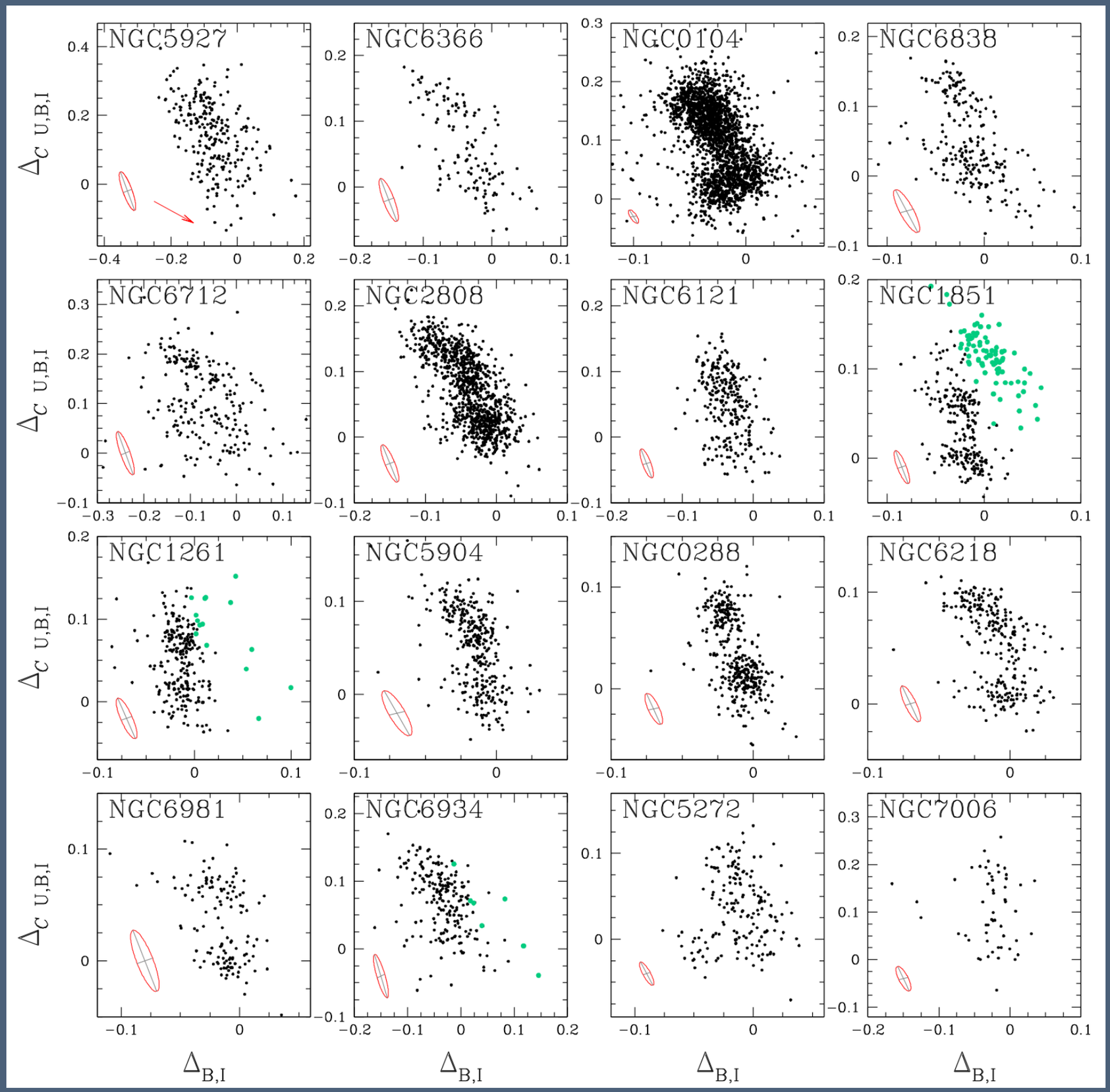

Results

1. identified bonafide cluster members and estimated the amount of differential reddening in the field of view of each cluster and found that the maximum reddening variation ranges from E(B–V) ~ 0.19 mag to less than 0.01 mag2

2. first time that ChMs are derived from ground-based Johnson–Cousin photometry

3. for NGC288 used the values of [O/Fe], [Na/Fe], and [Fe/H] (inferred by Carretta et al. 2009) from high-resolution spectroscopy to infer the chemical composition of the stellar populations identified on the ChM: 1G stars and 2G stars have the same iron abundance ($[Fe/H]_{2G–1G} = –0.01 \pm 0.01$). 2G stars are sodium, enhanced ($[Na/Fe]_{2G-1G} = 0.42 \pm 0.04$) and depleted oxygen depleted ($[O/Fe]_{2G–1G} = –0.28 \pm 0.09$) with respect to the 1G

4. shown that the U, B versus B, I ChM, which is derive by the I versus B – I and I versus U – B CMDs, provides a clear separation between 1G and 2G stars

Results

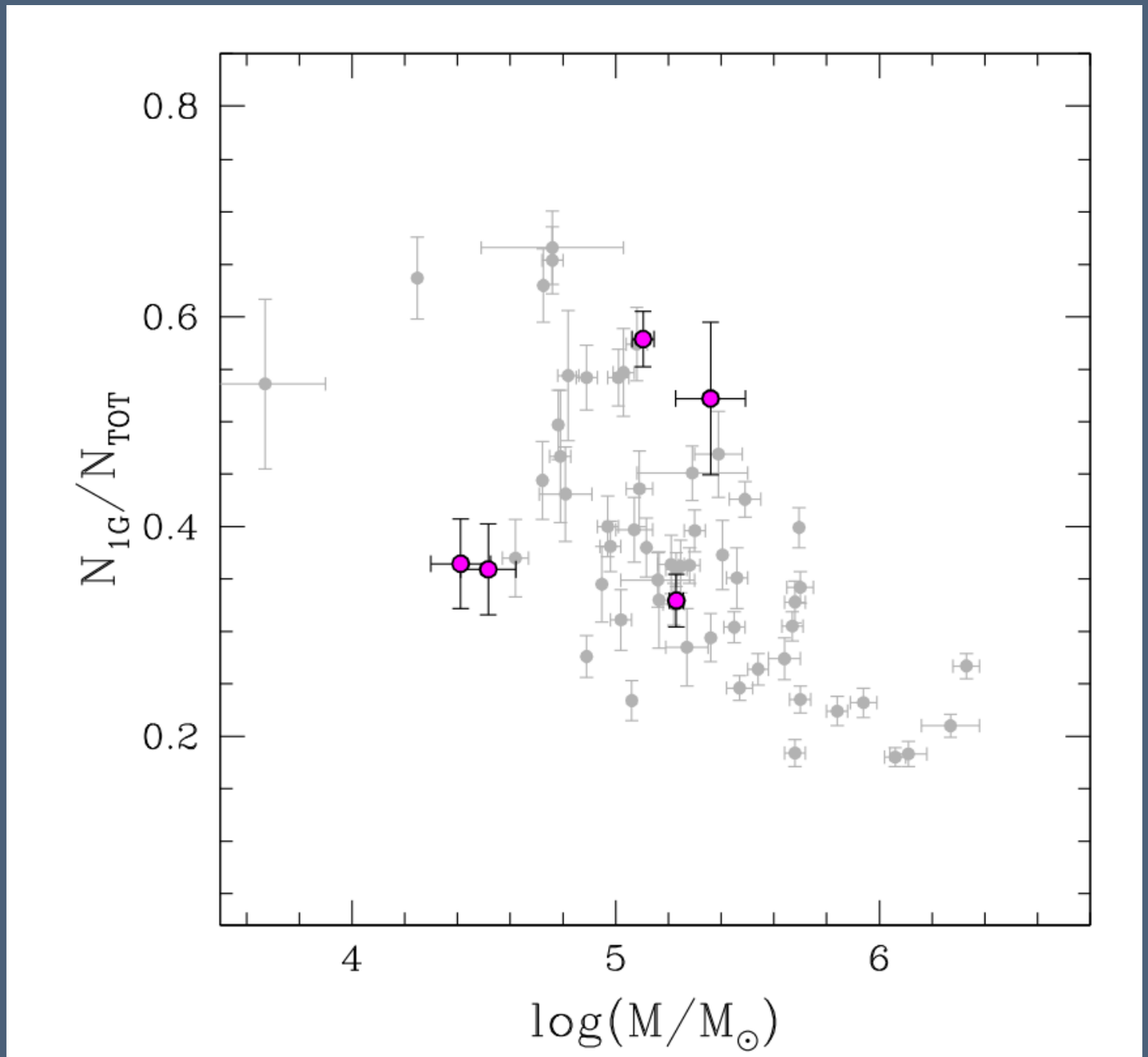

Figure 14. Fraction of 1G stars against the present-day cluster mass for Galactic GCs. Gray points indicate literature results (Milone et al. 2017a; Dondoglio et al. 2021), whereas magenta dots mark the clusters without previous studies on the ChM. Cluster masses are from Baumgardt & Hilker (2018).

Results

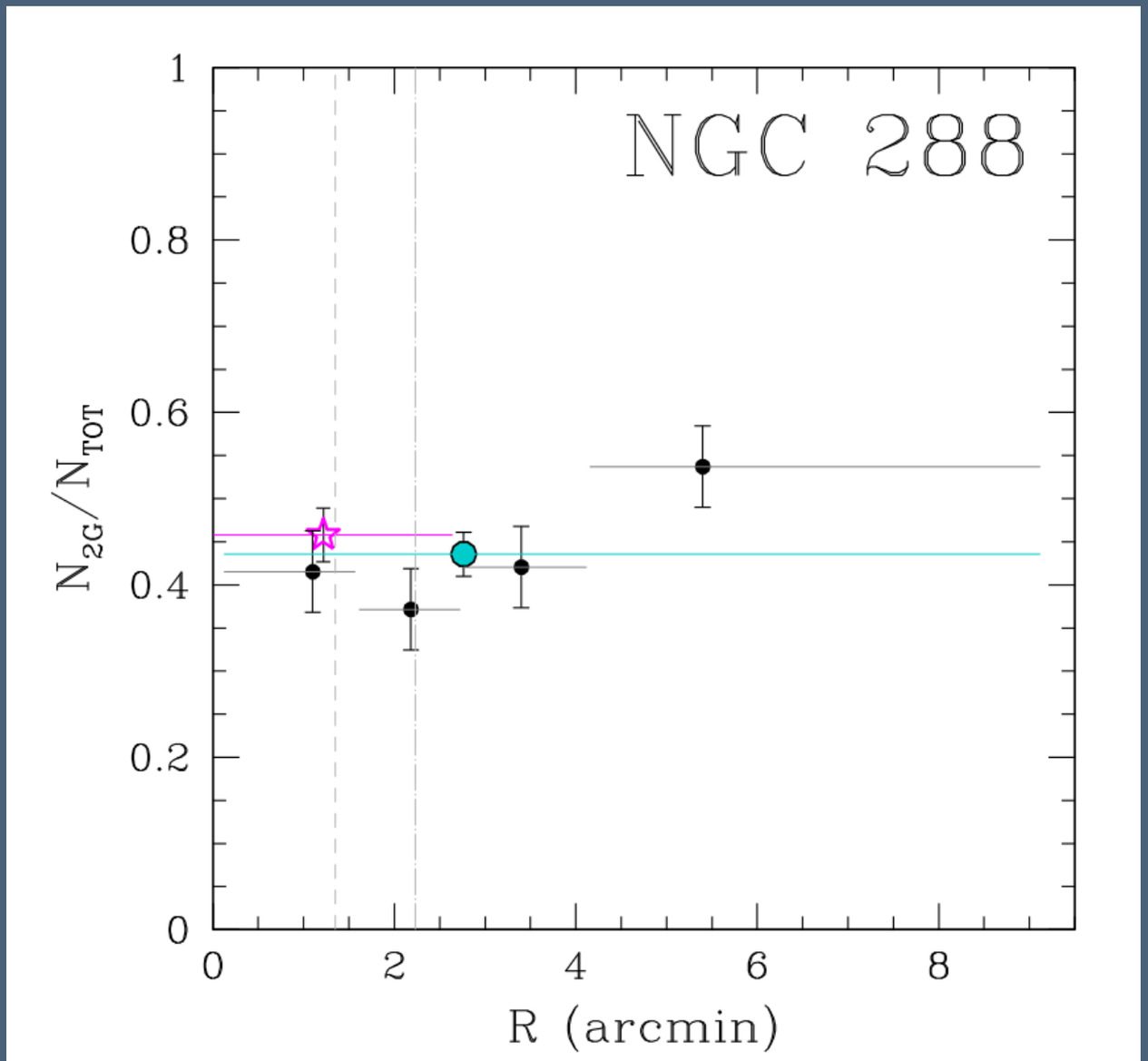

Figure 11. Fraction of 2G stars of NGC 288 against the radial distance from the cluster center. Black dots are derived in this paper, whereas the magenta starred symbol indicates the fraction of 2G stars measured by Milone et al. (2017a) from *HST* photometry. The cyan dot marks the average fraction of 2G stars from ground-based photometry. The horizontal segments mark the radial interval corresponding to each point. Vertical dotted and dashed–dotted lines indicate the core and half-light radius (from the 2010 version of the Harris 1996, catalogue).